

Logical fermions for fault-tolerant quantum simulation

Andrew J. Landahl^{1,2,3,*} and Benjamin C. A. Morrison^{1,2,3,†}

¹Center for Computing Research, Sandia National Laboratories, Albuquerque, NM, 87185, USA

²Center for Quantum Information and Control, University of New Mexico, Albuquerque, NM, 87131, USA

³Department of Physics and Astronomy, University of New Mexico, Albuquerque, NM, 87131, USA

We show how to absorb fermionic quantum simulation’s expensive fermion-to-qubit mapping overhead into the overhead already incurred by surface-code-based fault-tolerant quantum computing. The key idea is to process information in surface-code twist defects, which behave like logical Majorana fermions. Our approach encodes Dirac fermions, a key data type for simulation applications, directly into logical Majorana fermions rather than atop a logical qubit layer in the architecture. Using quantum simulation of the N -fermion 2D Fermi-Hubbard model as an exemplar, we demonstrate two immediate algorithmic improvements. First, by preserving the model’s locality at the logical level, we reduce the asymptotic Trotter-Suzuki quantum circuit depth from $\mathcal{O}(\sqrt{N})$ in a typical Jordan-Wigner encoding to $\mathcal{O}(1)$ in our encoding. Second, by exploiting optimizations manifest for logical fermions but less obvious for logical qubits, we reduce the T -count of the block-encoding SELECT oracle by 20% over standard implementations, even when realized by logical qubits and not logical fermions.

I. INTRODUCTION

In 1982, Richard Feynman famously argued that if we plan to simulate quantum mechanics with computers, then we should use *quantum* computers to do so [1]. He was right—quantum computers are expected to excel at simulating quantum systems, taking us far beyond the reach of conventional computers [2, 3]. In fields like quantum chemistry, materials science, nuclear physics, and high-energy physics, these systems are frequently comprised of *fermions* [4–10]. If the quantum computer simulating them uses *qubits* to store quantum information, then there is an unavoidable and substantial overhead required to map the fermions to the qubits [11]. Examples of such mappings include the Jordan-Wigner transformation [12], the Verstraete-Cirac transformation [13], the Bravyi-Kitaev transformation [14, 15] (and its “superfast” implementation via Fenwick trees [16]), and the ternary tree transformation [11]; see also Refs. [17–21]. Moreover, these qubits must have very low error rates for the results to be trustworthy. This means that the relevant qubits will likely need to be *logical* (*viz.*, encoded) qubits that are realized by quantum error correcting codes, and these codes must be processed using fault-tolerant quantum computing protocols, which adds even more overhead.

Feynmanian thinking suggests that we should use *fermionic* quantum computers to simulate fermionic systems. The fermionic quantum circuit model developed by Bravyi and Kitaev fits the bill [14]. In this model, elementary gates act as spacetime braids on the worldlines of Majorana fermions; any ordinary (Dirac) fermion can always be mathematically split into a pair of such Majorana fermions [22]. Realizing this model with physical

Majorana zero modes has been a decades-long quest that is still not complete, although progress continues to be made [23]. As an alternative, one can instead use “synthetic” Majorana fermions constructed from ordinary qubits arranged and processed with quantum surface codes [24, 25]. In these codes, “twist” defects in the lattice defining the codes act as *logical* Majorana fermions that are protected from noise [26–28]. By processing these logical Majorana fermions fault-tolerantly, there is an opportunity to eliminate the expensive fermion-to-logical-qubit mapping in the standard quantum software stack, as depicted in Fig. 1. In other words, it becomes possible to treat logical (Majorana) fermions as elementary data types that can be processed directly in fermionic quantum simulation algorithms. Hybrid algorithms that process logical qubits alongside logical fermions are also possible.

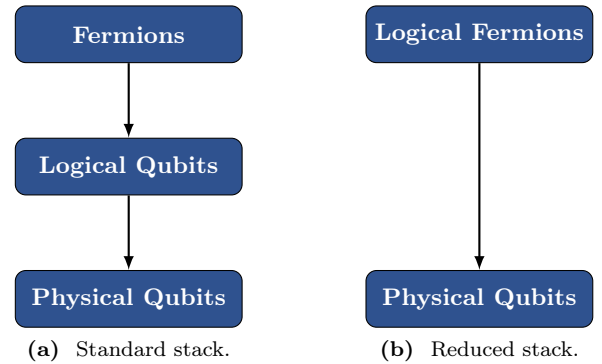


FIG. 1: Two choices for the fermion-to-qubit quantum software stack.

Embracing the logical (Majorana) fermion as an elementary data type for quantum computers is akin to embracing the floating point number, or *float*, as an elementary data type for classical computers. For machines that process qubits or bits at the lowest level, fermions or

*alandahl@sandia.gov

†benmorrison@unm.edu

floats might seem exotic. However, their existence belies the fact that many of the programs that we want to run on these computers naturally process these data types. Classical computers are even typically benchmarked by how many floating point operations per second (flops) they can achieve. Perhaps someday quantum computers will be benchmarked by how many fermionic operations per second they can achieve.

In this paper, we develop the reduced-stack architecture depicted in Fig. 1(b) and show how it can be exploited to deliver computational speedups for fermionic quantum simulation algorithms.

The remainder of this paper is organized as follows.

In Sec. II, we review the pertinent background on fermionic quantum circuits, logical fermion codes, and fermionic simulation algorithms. In Sec. III, we describe how to realize a logical fermionic architecture stack, compare it to the conventional error-corrected architecture for simulation, and examine how it can provide performance improvements in two exemplar systems. In Sec. IV, we conclude.

II. BACKGROUND

A. Majorana fermions and fermionic Hamiltonians

Consider a collection of fermions obeying the following canonical anticommutation relations on their elementary creation (f^\dagger) and annihilation (f) operators for modes labeled by a non-negative integer p :

$$\{f_p, f_q\} = \delta_{pq} \quad \{f_p, f_q\} = \{f_p^\dagger, f_q^\dagger\} = 0. \quad (1)$$

Because these relations discriminate between particles and antiparticles, we call them *Dirac* fermions.

One can always mathematically split a Dirac fermion into a pair of *Majorana* fermions. The corresponding elementary Majorana fermion operators are

$$c_{2p} := f_p^\dagger + f_p \quad c_{2p+1} := i(f_p^\dagger - f_p). \quad (2)$$

The induced Majorana fermion relations, which do *not* discriminate between particles and antiparticles, are

$$\{c_p, c_q\} = 2\delta_{pq} \quad c_p^\dagger = c_p. \quad (3)$$

Convenient derived fermionic operators include the *mode number operator*,

$$n_p := f_p^\dagger f_p = \frac{1}{2} \left(1 + i c_{2p} c_{2p+1} \right), \quad (4)$$

and the *total mode number operator*,

$$n := \sum_p n_p. \quad (5)$$

Fermionic Hilbert space, an example of a *Fock space*, is the completion of the infinite direct sum of antisymmetrized eigenspaces of n . Its standard basis is the set of

Fock states, which are states having definite eigenvalues for all n_p . The eigenvalues N_p for n_p are restricted to be 0 or 1 by the commutation relations, while the eigenvalue N for n can take on any non-negative integer value, or even be countably infinite.

Fermionic operators act on Fock state modes in a way that depends on the occupations of all previous modes, relative to some prescribed ordering of them:

$$f_p |\dots, N_p, \dots\rangle = (-1)^{\sum_{k=0}^{p-1} N_k} N_p |\dots, N_p - 1, \dots\rangle \quad (6)$$

$$f_p^\dagger |\dots, N_p, \dots\rangle = (-1)^{\sum_{k=0}^{p-1} N_k} (1 - N_p) |\dots, N_p + 1, \dots\rangle. \quad (7)$$

A *local* fermionic Hamiltonian is one that can be expressed as a sum of terms, each of which acts on Fock states in a way that depends only a constant number of fermionic modes. In order to avoid a dependence on the prescribed ordering used to label the fermion modes, local Hamiltonians have the feature that they only contain an even number of fermionic operators.

A final fermionic operator worth noting is the *total fermionic parity operator*,

$$Q := (-1)^n. \quad (8)$$

Because each term in a local Hamiltonian H acts on an even number of modes, it necessarily obeys $[H, Q] = 0$, conserving total fermionic parity. Such a Hamiltonian might or might not also obey $[H, n] = 0$. If it does not obey this, then the total mode number is not conserved. This is the case for Hamiltonians that include BCS-like interactions [29, 30] of the form

$$\sum_{p,q} (f_p f_q + f_q^\dagger f_p^\dagger). \quad (9)$$

In terms of Majorana fermion operators, the most general form of an N -mode local fermionic Hamiltonian with only one-body and two-body interactions is

$$H = \sum_{p,q=0}^{2N-1} h_{pq} c_p c_q + \sum_{p,q,r,s=0}^{2N-1} g_{pqrs} c_p c_q c_r c_s, \quad (10)$$

where the h_{pq} and g_{pqrs} are real coefficients. This is the class of fermionic Hamiltonians we will show how to simulate fault-tolerantly.

B. The Jordan-Wigner transformation

As noted in Sec. I, mapping fermions to qubits is a task that necessarily incurs a non-negligible overhead. The reason for this essentially boils down to the fact that the commutation algebra of qubit Pauli operators is much different than that of fermions. Pauli operators can anticommute on the same qubit, but they always commute on different qubits. On the other hand, fermion creation

and annihilation operators anticommute even when they act on different modes.

While there are many fermion-to-qubit mappings, as noted in Sec. I, two general paradigms can be considered. When n fermions are represented with n qubits, as in [11, 12, 14, 15], annihilation and creation operators cannot be asymptotically local; on average, each fermionic operator must be mapped to a qubit operator acting on at least $\log_3(2n)$ qubits, if the fermionic algebra is to be represented faithfully [11]. Alternatively, for lattices and other systems with limited connectivity, that structure can be exploited to allow constant-weight fermionic operators to be mapped to constant-weight fermionic operators. However, this requires a number of additional qubits that scales with the connectivity of the target system [13, 16–21, 31]. Hybrids between these approaches are also possible [32], with some of the advantages of each but still dependent on limited connectivity to be efficient.

While the ternary tree mapping [11] nearly saturates the $\log_3(2n)$ bound for a general-purpose mapping, we describe the asymptotically less efficient, but simpler, Jordan-Wigner transformation [12] here instead. Our reason for doing this is that, at the logical Majorana fermion level, the reduced-stack architecture we explore shares many similarities with this transformation.

In the Jordan-Wigner transformation, the fermion creation and annihilation operators for mode p in an N -fermion system are represented by weight- p Pauli operators on qubits $0, \dots, N-1$ as follows:

$$f_p = \frac{1}{2}(Z_0 \otimes \dots \otimes Z_{p-1}) \otimes (X_p + iY_p) \quad (11)$$

$$f_p^\dagger = \frac{1}{2}(Z_0 \otimes \dots \otimes Z_{p-1}) \otimes (X_p - iY_p). \quad (12)$$

Somewhat more simply, the corresponding Majorana fermion operators are mapped as follows under the Jordan-Wigner transformation:

$$c_{2p} = (Z_0 \otimes \dots \otimes Z_{p-1}) \otimes X_p \quad (13)$$

$$c_{2p+1} = (Z_0 \otimes \dots \otimes Z_{p-1}) \otimes Y_p. \quad (14)$$

Inverting this mapping yields

$$X_p = (-i)^p c_0 \dots c_{2p} \quad (15)$$

$$Z_p = -i c_{2p} c_{2p+1}. \quad (16)$$

Notably, the operators that map to single-site Pauli X operators are odd-weight Majorana operators, which do not preserve Q , the global fermionic parity.

C. Majorana fermionic quantum circuits

In the standard Majorana fermionic quantum circuit (MFQC) model of quantum computation [14], solving a computational problem is a three-step process:

1. Use a classical computer to select a quantum circuit from a P -uniform family of Majorana fermionic quantum circuits [33].
2. Execute the MFQC on a quantum computer.
3. Return the classical result, say, as a bit string.

In this process, each MFQC in the family is expressible as a sequence of elementary operations on a collection of Majorana fermions. The elementary operations include preparations, measurements, and quantum coherent operations. Here, as is common, we restrict our attention to circuits in which each elementary operation acts on only a constant number of operands. Generally, to ensure that elementary Majorana operations can be generated by local Hamiltonians, they are restricted to act on only even numbers of Majorana fermions, which ensures global fermionic parity preservation. However, we will only consider elementary operations that act on two or four Majorana fermions at a time. If the set of elementary operations can be used to approximate any parity-preserving transformation on the Majorana fermions arbitrarily well by a sufficiently long circuit, then the set of operations is said to comprise a universal gate set. (We use the term “gate set” even when the set contains not just coherent gates but also preparation and measurement operations.)

In their landmark paper defining the standard MFQC model [14], Bravyi and Kitaev presented several universal gate sets. The one we consider realizing here with logical Majorana fermions is one of these, adapted by Li in Ref. [34] so that it uses only preparations, measurements, and Majorana exchanges on a collection of Majorana fermions indexed by the variables p, q, r , and s . The fact that exchanging Majoranas can implement nontrivial gates is related to the fact that Majoranas are a model of Ising anyons, which are particles that interact topologically in $(2+1)$ spacetime dimensions. For more details on the connection to topological quantum computing, including the connection between Majorana fermions and Ising anyons, see, for example, the textbooks by Wang [35] and Pachos [36].

1. Prepare a $+1$ eigenstate of the *Majorana fusion* operator, sometimes also called the *Majorana exchange* operator, $F_{pq} = ic_p c_q$. This operator is closely related to, but not the same as, the mode number operator of Eq. (4).
2. Measure the two-fermion observable F_{pq} (either destructively or non-destructively.¹).
3. Measure the four-fermion observable $F_{pq} F_{rs}$ non-destructively.

¹ By “non-destructive,” we mean that the post-measured quantum state is an eigenstate of the observable measured, as per the standard von Neumann prescription [37]. In a destructive measurement, only the classical measurement outcome remains.

4. Prepare the “magic state” $|T\rangle_{pqrs}$, which is the $+1$ eigenstate of the following observables:

$$F_{pq}F_{rs} \quad (17)$$

$$\frac{F_{pq} + F_{pr}}{\sqrt{2}}. \quad (18)$$

5. Apply the (unitary) Majorana exchange gate F_{pq} .

By using Majorana exchange frame tracking [38], reminiscent of Clifford frame tracking for qubits [39, 40], one can dispense with the final coherent gate in the Li gate set, converting the gate set into one comprised solely of measurement and preparation operations. This basis allows one to realize measurement-based universal topological quantum computing [38, 41–43] in a fashion reminiscent of fusion-based quantum computing [44]. Fig. 2 depicts an example of a Majorana fermion circuit that implements the coherent Majorana exchange gate F_{ps} using only non-destructive two-fermion measurements.

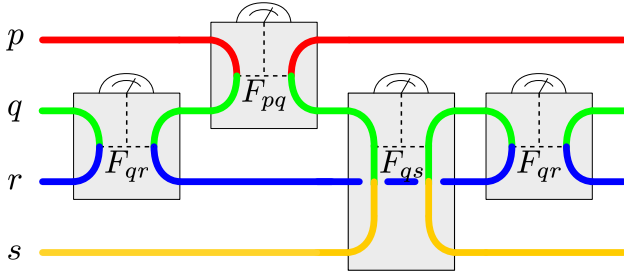


FIG. 2: (Color online.) A fermionic quantum circuit for realizing the coherent counterclockwise exchange F_{ps} of Majorana fermions using only non-destructive measurements on pairs of Majorana fermions. The information is exchanged between the Majorana fermion modes labeled p , q , r , and s , even though the carriers themselves are not exchanged (indicated by colored worldlines moving from left to right). Generally, the measurement of the fusion operators can yield non-trivial outcomes, which can be handled by adaptive logic, such as with a “forced measurement” protocol [41] or “Majorana frame tracking” [38]; the circuit depicted here imagines that all fusion measurement outcomes are trivial.

D. Majorana fermion stabilizer codes

A *Majorana fermion stabilizer code* [45], or Majorana stabilizer code for brevity, is the simultaneous $+1$ eigenspace of a collection of commuting, Hermitian, even-weight Majorana operators. The evenness constraint ensures that these operators are fermion-parity preserving, and hence physically observable. Following the language used for qubit stabilizer codes [46], we say these operators generate the code’s *stabilizer group*, and each operator is called a *stabilizer generator*, or sometimes just a *stabilizer* or a *check* for brevity, because they “stabilize” the codespace and are what are measured to “check” for errors. More generally, in a *subsystem* Majorana stabilizer

code, the measured checks need not commute and the stabilizer group is defined to be the center of the *check group*. Whether for subspace or subsystem Majorana stabilizer codes, the *logical group* is the check group’s normalizer.

Without loss of generality, each check in a Majorana stabilizer code can be written as S_σ , where σ indicates the set of modes V_σ on which it has support. Each logical operator L is supported on a set of modes V_L obeying $|V_L \cap V_\sigma| \equiv 0 \pmod{2}$ for each σ to ensure that the logical group and stabilizer group commute. Mathematically, each check and logical operator can be expressed as

$$S_\sigma := i^{|V_\sigma|/2} \prod_{q \in V_\sigma} c_q \quad (19)$$

$$L := \eta_L \prod_{q \in V_L} c_q, \quad (20)$$

where $\eta_L \in \{\pm 1, \pm i\}$ is a phase.

The *distance* of a Majorana fermion stabilizer code is the minimum nonzero weight of its logical group’s elements. Unlike qubit codes, a Majorana fermion stabilizer code of distance d cannot necessarily correct all Majorana errors of weight $\lfloor (d-1)/2 \rfloor$ or less, because the codes treat even and odd logical operators on the same footing, exposing them, *e.g.*, to “quasiparticle poisoning” errors from weight-one Majorana fermion operators, which do not conserve fermionic parity locally, but might do so when the environmental degrees of freedom of the bath are taken into consideration [47]. With clever concatenation techniques, this can be avoided, as will be discussed later.

A *fermion stabilizer code* is a Majorana stabilizer code on an even number $(2n)$ of Majorana fermions [45, 47]. One can show that a fermion stabilizer code’s logical group is isomorphic to the Pauli group on $k = n - |\{S_\sigma\}|$ logical qubits, so that one can think of such codes as encoding k logical qubits in $2n$ physical Majorana fermions [45]. Following Ref. [47], we use $\llbracket n, k, d \rrbracket_f$, or alternatively $\llbracket 2n, k, d \rrbracket_m$, to denote a fermion stabilizer code that encodes k qubits to distance d in n Dirac fermions, or equivalently, in $2n$ Majorana fermions.

A *Majorana surface code* is a Majorana stabilizer code defined by an embedding of a graph into a surface. Generally, one can use a rotation system to define such codes [48]. Here, we only need to consider a subclass of Majorana surface codes, first described by Litinski and van Oppen [49], that are defined by face-three-colorable graphs embedded on a disk in which one associates Majorana fermions with vertices and checks with faces. (The “face” outside the graph in the disk might not be able to be consistently colored with all the other faces [48].)

E. Majorana cycle codes

A *Majorana cycle code* is a $\llbracket n+1, n, 2 \rrbracket_f$ Majorana surface code defined by a $(2n+2)$ -vertex cycle graph embedded on a disk. Each Majorana cycle code has a single

check, corresponding to the product of all of the Majorana fermion operators on the vertices, up to a phase consistent with Eq. (19). The constraint that the codes are $+1$ eigenstates of this check operator is just the even-parity constraint required of any collection of indistinguishable fermions.

There are many ways of choosing logical Pauli operator bases for these codes. The simplest nontrivial Majorana cycle codes are called the *tetron code* and the *hexon code*, encoded into four and six Majorana fermions respectively [49–51]. For the tetron code, we choose the logical operator basis to be

$$\bar{X} = -ic_0c_1 \quad \bar{Z} = -ic_1c_2. \quad (21)$$

We include overall minus signs in the η_L phases used in these definitions to make the relationship between this encoding and the inverse Jordan-Wigner transformation in Eqs. (15)–(16) clearer. The stabilizer group for this code is generated by a single element, which from Eq. (19) is

$$S = -c_0c_1c_2c_3. \quad (22)$$

For the hexon code, we choose the logical operator basis to be

$$\bar{X}_0 = -ic_0c_1 \quad \bar{Z}_0 = -ic_1c_2 \quad (23)$$

$$\bar{X}_1 = -c_0c_1c_2c_3 \quad \bar{Z}_1 = -ic_3c_4, \quad (24)$$

with a stabilizer group generated by the operator

$$S = -ic_0c_1c_2c_3c_4c_5. \quad (25)$$

These choices are captured in Fig. 3.

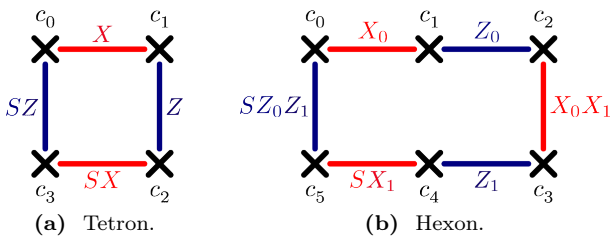


FIG. 3: (Color online.) Logical operator bases for some simple Majorana cycle codes.

Generally, we choose the logical operator basis for a Majorana cycle code to be

$$\bar{X}_p = (-i)^{p+1}(c_0 \dots c_{2p+1}) \quad (26)$$

$$\bar{Z}_p = -ic_{2p+1}c_{2p+2}. \quad (27)$$

This choice is depicted diagrammatically in Fig. 4.

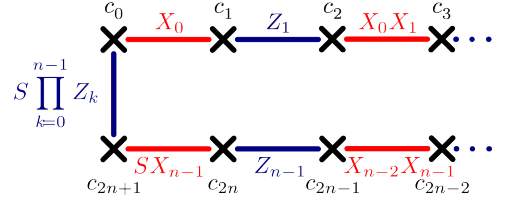


FIG. 4: (Color online.) Logical operator basis for a general Majorana cycle code.

The Majorana cycle code is a Jordan-Wigner-like code; it differs from the inverted Jordan-Wigner transformation described in Eqs. (15)–(16) by the addition of two extra Majorana fermions. These serve to ensure that every \bar{X}_p preserves global fermionic parity: each logical \bar{X}_p now acts on one more Majorana mode, giving it even weight, and each of the logical \bar{Z}_p operators is defined on a pair of Majorana modes that are shifted by one relative to the inverse Jordan-Wigner transformation to accommodate this. Notice that the logical operators defined on the mode c_{2n+1} are elusive. The X -like and Z -like logical operators defined on them are equivalently expressed as a product of all of the other X -like and Z -like logical operators, respectively, up to multiplication by the lone stabilizer generator.

A large Majorana cycle block code like the one depicted in Fig. 4 is nearly twice as efficient at encoding qubits as a collection of tetron block codes combined via a tensor product, which yield effectively only a $[[2n, n, 2]]_f$ code. For this reason, and to simplify our constructions later, we only consider encodings into large Majorana cycle block codes [52]. We discuss how to move between these encodings in Appendix B.

F. Logical Majorana codes

Like Majorana surface codes, qubit surface codes [24, 53–59] can be defined using a rotation system that describes a graph embedding combinatorially [48]. As with Majorana surface codes, we will only consider a narrow subclass of such codes, namely those defined by face-two-colorable (“checkerboardable”) graphs containing squares and digons embedded on a disk in which one associates qubits with vertices and checks with faces. (The “face” outside the graph in the disk might not be able to be consistently colored with all the other faces [48].) A check of one face color can be associated with a tensor product of Pauli X operators on its incident qubits; a check of the other face color can be associated with a tensor product of Pauli Z operators on its incident qubits. Alternatively, all checks can be given the same local structure by a set of local basis changes, turning it into a so-called $XZZX$ code [60]. Because these qubit surface codes are embedded on a disk, we call them qubit surface-code patches.

The number of logical qubits encoded by a surface code

patch is related to its number of boundary components, where each boundary component can be associated with a logical operator, as described in Ref. [28]. Because of this, the perimeter can be described by a cycle graph, in exactly the same way that Majorana cycle codes are described. The locations where the boundary type changes are called *corner twists*, following terminology used in Refs. [26–28, 61–69]. Examples of surface-code patches with perimeters that can be described by the C_4 (tetron) and C_6 (hexon) cycle graphs are depicted in Fig. 5.

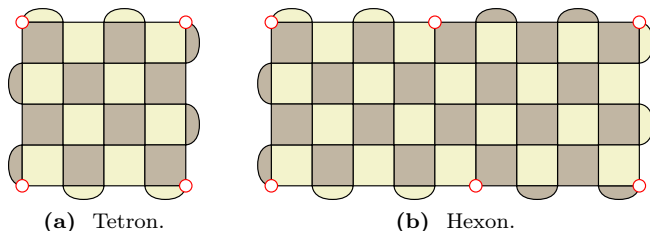


FIG. 5: (Color online.) Distance-five versions of surface code patches that realize logical Majorana fermions as “corner twist defects,” depicted by white circles with red boundaries.

The similarity between the codes in Fig. 3 and Fig. 5 is not mere coincidence. The corner twist defects act like logical Majorana fermions (or, more precisely, like \mathbb{Z}_2 -crossed braided tensor categories [67]), as pointed out in Refs. [26–28]. In other words, these codes essentially encode logical Majorana fermions in physical qubits. To disambiguate from the term “Majorana fermion code,” which describes a code that works the other way around by encoding physical Majorana fermions into logical qubits [34, 45, 47, 49, 51, 54, 70–72], we will call these *logical Majorana fermion codes*, or just *logical Majorana codes*, for short.

Upon closer examination, one can see that the logical Majorana operators for the tetron and hexon qubit surface codes are themselves further encoded in the tetron and hexon codes, respectively. These qubit surface-code patches are therefore *concatenated* codes, in which physical qubits realize logical Majorana fermions, which in turn realize logical qubits. A helpful consequence is that quasiparticle poisoning errors are not a concern, because errors on physical qubit-level operations, once decoded with the lower-level logical Majorana code, translate at worst to even-weight logical Majorana operators in the upper-level tetron or hexon code. This means that a distance- d qubit tetron or hexon surface code protects its encoded logical Majorana fermions against all physical errors of weight $\lfloor (d-1)/2 \rfloor$ or less. These properties hold for the straightforward generalization to general qubit surface-code patches that are associated with Majorana cycle codes.

G. Fault-tolerant surface-code computation with logical Pauli measurements and preparations

In the ordinary qubit quantum circuit model, there is a universal gate basis that consists solely of one- and two-qubit preparations and measurements on pairs of qubits (labeled p and q) that is similar to the Li gate basis described in Sec. II C. The gate basis is as follows:

1. Prepare a $+1$ eigenstate of the Pauli operators X_p and Z_p .
2. Measure the Pauli operators X_p and Z_p (either destructively or non-destructively).
3. Measure the Pauli operators $X_p X_q$ and $Z_p Z_q$ non-destructively.
4. Prepare the “magic state” $|T\rangle_p$, which is the $+1$ eigenstate of the following observable:

$$\frac{X_p + Z_p}{\sqrt{2}}. \quad (28)$$

Although logical Pauli operators can be represented by simple strings of physical Pauli operators between twists in the surface code, measuring and preparing these operators fault-tolerantly is not as simple as just measuring or preparing the qubits along the relevant strings, because the individual qubit operations might be faulty. Nevertheless, several fault-tolerant protocols for realizing these exist. Here, we review one preparation protocol [73] and three measurement protocols: one based on interior twist braiding [27], one based on corner twist lattice surgery [40], and one based on twist teleportation via “portal pairs” [69].

A helpful primitive for all of these protocols is a fault-tolerant procedure for bringing corner twists to the interior (and vice versa) of surface code patches; one way of doing this is described in detail in Ref. [27]. Interior twists come in one of two varieties. An interior twist can either be a disclination (rotational) twist or a dislocation (translational) twist. Either type causes the colorability of plaquettes in the surface-code lattice to be frustrated; the latter have a convenient representation that does not disturb the locations of vertices in the lattice, so we will focus our attention on this type for pedagogical clarity.

A small interior dislocation twist can be represented by a weight-five $XXYZZ$ check that spans the space that two ordinary weight-four $XXXX$ and $ZZZZ$ checks would have occupied. The code distance of the associated logical qubit represented by this twist is the minimum of the perimeter of the twist (in this case, five) and the distance of the twist to the nearest other twist. Manifestly, then, a code with just a single twist cannot encode a logical qubit. The code distance can be increased by removing adjacent checks to the twist and separating it farther away from other twists. Pairs of twists can be connected by “defect lines,” which connect the qubits in each twist on which the Y operator has support along a

collection of qubits that have been removed from the lattice to accommodate the twist; Fig. 6 depicts an example of two weight-five interior twists whose separation from each other is just three qubits apart.

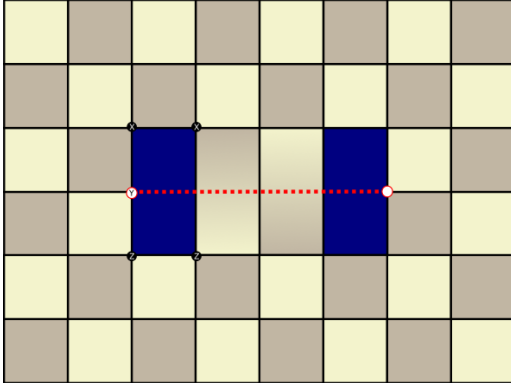


FIG. 6: (Color online.) A logical qubit implemented as a pair of dislocation twist defects, represented by “missing” $XXYZZ$ checks.

Most fault-tolerant preparation protocols for logical qubits in the surface code focus on preparing a single logical qubit in the tetron surface code. This is because, in principle, preparations for isolated tetron surface codes can be combined by first bringing the corner twists into the interior as puncture defects, and then stitching them together via lattice surgery, as described, for example, in Refs. [73–75]. The preparation protocol for a single tetron is fairly simple: one prepares all physical qubits in the eigenstate of the desired Pauli operator, X or Z , and then performs fault-tolerant syndrome extraction on the qubits. One way to prepare a low-fidelity version of the magic state (to “inject it” into the code), as described in Ref. [73], is to first prepare four mini-patches, one in each quadrant, surrounding a physical qubit prepared in the $|T\rangle$ state. Then one measures the checks three times and performs fault-tolerant decoding on the result. Although this only suppresses errors to second-order in the errors of the physical operations, the preparation of the physical $|T\rangle$ state itself is only good to first-order in this error. The resultant low-fidelity state can be distilled to any desired precision (limited by the code distance) by any of a number of magic-state distillation protocols, such as the Bravyi-Kitaev protocol [76], using the other fault-tolerant operations in the universal set.

Ref. [27] describes a protocol for how to measure a logical qubit represented by a pair of interior twists. In the protocol, one entangles the twist pair with an auxiliary logical qubit represented by a pair of (non-twist) punctures (*viz.*, missing connected check regions). The protocol requires braiding one of the punctures around the twist pair by a sequence of internal code deformations, followed by destructively measuring the auxiliary logical puncture pair that represents the logical qubit. Indeed, this protocol can be used to measure the product of any number of logical qubits stored in an even number of

twists, simply by braiding the punctures along the correct path. This protocol requires a greater separation between twists than the other two alternatives we describe next, because it is necessary to leave space for the punctures to move around without compromising the distance of the code. However, it doesn’t require any unusual hardware features beyond the ability to turn particular stabilizer generators on and off.

By moving all interior twists to corner twists on the boundary, one can measure an arbitrary logical Pauli product operator using the lattice-surgery protocols described in Ref. [40]. However, this occupies a length of the surface code’s perimeter that is proportional to the number of twists being measured. One challenge with this protocol is the limitations on parallelism it imposes if all logical qubits are confined to a single patch, such as in a large logical Majorana fermion code when thought of as a logical-qubit code. In this case, for example, in order to measure $\Theta(n)$ quadratic Majorana (single-logical-qubit) or quartic Majorana (two-logical-qubit) operators on n twists in parallel, one needs a surface code patch with perimeter at least $\Omega(dn)$, where d is the distance of the code. While this is possible with a narrow rectangular patch with twists arranged in a $2 \times \frac{n}{2}$ array, achieving it on the square-lattice arrays of twists that match the geometry of simulation targets (and thus support the speedups described in this paper) requires a patch with highly unconventional structure. A notable advantage, however, is the ease of $|T\rangle$ state injection at the boundary, allowing the use of external T -factories rather than needing to locate them within the main computational patch, as described in Ref. [40].

Finally, Ref. [69] describes “portal pairs” that can be used to teleport twists to a future time, allowing direct non-destructive measurements of any twist operator in a number of rounds equal to the code’s distance. This allows the most compact array of twists, as no physical braiding or movement of twists whatsoever is required. However, it requires highly nonlocal physical operations, potentially even in time as well as in space, and as a result is only suited to very specific hardware models: in its original conception, a photonic architecture [77] with a fiber delay line.

H. Trotter-Suzuki approximation

For simulation applications run on quantum computers, a common target is the implementation of time-evolution operator

$$U = e^{-itH} \quad (29)$$

corresponding to a physical Hamiltonian H . While this operator is unitary, and thus at least theoretically possible to implement on a quantum computer, it may be extremely difficult to implement exactly in practice. Accordingly, several methods have been proposed for approximate implementations of U ; here we discuss the

Trotter-Suzuki decomposition [78]. It requires the Hamiltonian be written as a sum of Trotter layers H_L , where each layer is a sum of commuting terms that do not necessarily commute with the terms in other layers. The exponentiated Hamiltonian

$$U = e^{-itH} = e^{-it \sum_L H_L} \quad (30)$$

is then approximated as

$$\tilde{U} = \prod_L e^{-itH_L}. \quad (31)$$

For practicality of implementation, we will further decompose each Trotter layer H_L into a sum of sub-layers, grouping the Pauli products or even-weight Majorana fermionic operators more finely than the commutation relations would require. Each of these “Pauli product layers” or “Majorana layers” should consist only of terms that are supported on disjoint sets of information carriers (qubits or fermions, respectively), so that the gates within an exponentiated layer can be implemented in parallel. Because those sub-layers commute with each other, the sub-decompositions are exact and do not introduce any additional approximation error into the simulated evolution. The resulting circuit depth is proportional to the number of Pauli product layers or Majorana layers.

In fault-tolerant quantum computing architectures, it is common that the fault-tolerant realizations of non-Clifford gates are more costly, in terms of physical resources like physical qubits and time, than fault-tolerant realizations of Clifford gates [79]. For this reason, it is also common to synthesize all fault-tolerant quantum circuits so that they depend on only one, or only a few, types of non-Clifford gates, such as the T gate, which is the fourth-root of the Pauli Z gate. A proxy for the complexity of fault-tolerant circuits is then the T count, which counts the number of T gates in a quantum circuit.

The T count is unaffected by the choice of Trotter layering, although related measures, such as the T depth, which is the circuit depth of T gates utilized, may be affected by the choice of Trotter layering. While T gates might require many gates to be synthesized fault-tolerantly, say through one or more “magic state factories,” the total runtime of the quantum algorithm is not necessarily impacted by this cost because, with sufficiently many factories, “magic” $|T\rangle$ states can be supplied with high fidelity on demand whenever a T gate is required [40]. Hence, for the purposes of determining the overall runtime of the fault-tolerant quantum algorithm, one can assign a depth cost of one to T gates.

Another useful measure of circuit complexity is the overall gate count utilized. This dictates the size of quantum error correcting code required, because larger circuits require larger codes to maintain fault tolerance.

I. Block encoding for Hamiltonian simulation

Block-encoding methods [80] have been proposed as an alternative to Trotter-Suzuki decomposition for simulation of the Fermi-Hubbard model and other quantum systems [81].

For concreteness, consider a Hamiltonian H that is expressible as a linear combination of Hermitian unitary operators H_ℓ with real coefficients w_ℓ (which, without loss of generality, we take to be positive by absorbing minus signs into the H_ℓ terms). In other words, consider the Hamiltonian

$$H = \sum w_\ell H_\ell \quad \text{s.t.} \quad w_\ell \in \mathbb{R}, \quad w_\ell > 0, \quad H_\ell^2 = \mathbb{1}. \quad (32)$$

From this Hamiltonian, one can construct a pair of oracle circuits. PREPARE prepares a superposition $|\mathcal{L}\rangle$ of indices $|\ell\rangle$ that specify Hamiltonian terms, with coefficients proportional to the corresponding terms’ coefficients w_ℓ in the Hamiltonian:

$$\text{PREPARE } |0\rangle = \sum \sqrt{\frac{w_\ell}{\lambda}} |\ell\rangle = |\mathcal{L}\rangle, \quad (33)$$

where $\lambda := \sum |w_\ell|$. SELECT applies a Hamiltonian term H_ℓ specified by an index register onto a system register:

$$\text{SELECT} = \sum_\ell |\ell\rangle \langle \ell| \otimes H_\ell. \quad (34)$$

These oracles together satisfy the “qubitization” relation

$$(\langle \mathcal{L}| \otimes \mathbb{1}) \text{SELECT} (|\mathcal{L}\rangle \otimes \mathbb{1}) = \frac{1}{\lambda} \sum_\ell w_\ell H_\ell = \frac{H}{\lambda}, \quad (35)$$

which means that we can encode the desired spectrum into an associated “quantum walk” operator \mathcal{W} by defining \mathcal{W} as

$$\mathcal{W} = (2 |\mathcal{L}\rangle \langle \mathcal{L}| \otimes \mathbb{1} - \mathbb{1}) \text{SELECT}. \quad (36)$$

In other words, on the subspace spanned by $|\mathcal{L}\rangle|k\rangle$ and the component of $\mathcal{W}|\mathcal{L}\rangle|k\rangle$ that is orthogonal to $|\mathcal{L}\rangle|k\rangle$, the quantum walk operator acts as

$$\mathcal{W} = e^{iY \arccos(E_k/\lambda)}, \quad (37)$$

where Y is the Pauli Y operator and E_k is the k -th eigenvalue of H . To find the eigenvalues of H , then, it suffices to instead find the eigenvalues of \mathcal{W} .

To perform phase estimation on this operator, we will need to implement a controlled version of it, which can be done via the following circuit if PREPARE, PREPARE † , and controlled-SELECT are available.

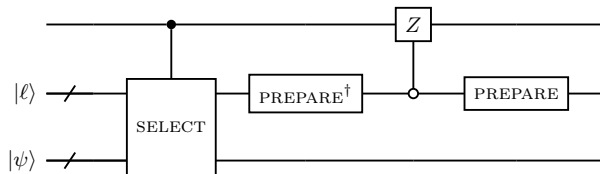


FIG. 7: The controlled qubitized walk operator $\Lambda(W)$.

The controlled walk operator must be applied $\mathcal{O}(\lambda/\Delta E)$ times, where ΔE is the desired error bound on the ground state energy.

J. Fermi-Hubbard model system and Hamiltonian

In order to demonstrate the techniques we develop herein, we require an exemplar system to simulate. For the sake of simplicity and ease of application, we will consider the planar Fermi-Hubbard model for each demonstration.

The Fermi-Hubbard model describes a many-electron system on a lattice; we consider specifically the case of a two-dimensional square lattice. While originally constructed to describe correlation effects in the d -band of a transition metal [82], under the approximation of a narrow band with nearest-neighbor and on-site interactions only, it has more recently been applied to modeling cuprate superconductors [83]. The model Hamiltonian consists of a hopping term and an on-site self-energy term

$$H_{\text{HUB}} = -t \sum_{\langle p,q \rangle, \sigma} a_{p,\sigma}^\dagger a_{q,\sigma} + \frac{u}{2} \sum_{p, \alpha \neq \beta} n_{p,\alpha} n_{p,\beta} \quad (38)$$

where p and q index lattice sites, σ , α , and β index spins, $\langle p, q \rangle$ indicates a sum over pairs of adjacent lattice sites only, and t and u parametrize the interaction strengths. Simulations of the model typically consider a finite lattice with N sites, before extrapolating results to infinite systems (and the thermodynamic limit more generally) [83].

Approximate solutions to the Fermi-Hubbard model—obtained via classical algorithms including Monte Carlo, embedding methods, density matrix renormalization group theory, coupled-cluster methods, and multi-reference Hartree-Fock—show ferromagnetism, superconductivity, and metal-insulator transitions, depending on Hamiltonian parameters [83]. This combination of varied behavior and simplicity makes it a valuable test environment for fermion simulation techniques [81].

Prior work has examined the Fermi-Hubbard model for simulation on quantum computers in both the Trotter-Suzuki [84] and qubitization [81] paradigms. The Trotterized implementation considered a NISQ architecture, with the controlled- i SWAP as a fundamental gate [84]; their resource estimates, accordingly, will not be directly comparable with ours. Thus, in Sec. III B we will make

resource estimates both with and without logical Majorana fermion techniques. The qubitized implementation [81] considers a similar fault-tolerant paradigm to the one we work in, however, so we will reference their resource estimation for comparison to our own.

The qubitized approach to simulation relies on repeated application of a pair of block-encoding oracles, PREPARE and SELECT, as specified in Eq. (33) and Eq. (34). These two oracles can be implemented with costs $\mathcal{O}(\log N)$ and $10N + \mathcal{O}(\log N)$ respectively for the N -site Fermi-Hubbard model [81], which we will take as an “industry standard” to compare our Majorana-fermion-inspired block encoding oracles to in Sec. III C.

III. RESULTS

Surface code patches can encode logical qubits via the inclusion of twist defects in their structure. However, when acting on those twist defects directly rather than via the abstraction of logical qubit constructions, they support Majorana fermionic operations; that is, the surface code patches encode logical Majorana fermions in their twist defects, and it is natural to think of them as logical Majorana codes, as described in Sec. II F. Here, in Sec. III A, we show how one can realize a universal set of operations drawn from the fermionic quantum circuit gate basis described in Sec. II C on these logical Majorana fermions. Logical Majorana fermions can then serve as a new logical data type, together with its own set of logical operations, for use in fault-tolerant fermionic simulation algorithms.

Many applications of quantum computing require the implementation of Dirac fermionic operators. Traditionally, the Jordan-Wigner or another encoding is used to encode Dirac fermions into qubits (Sec. II B). On a surface-code-based fault-tolerant quantum computer, this means that there is a stack of abstraction layers from Dirac fermions to logical qubits to surface code twist defects to physical data qubits, shown in Fig. 8(a). The twist defect layer is usually elided from descriptions of the surface code architecture. However, as described in Sec. II F, the color-changes on the boundaries of surface code patches have similar properties to internal twist defects and so are called *corner twists* [26–28, 61–69], and in turn act like logical Majorana fermions [26–28]. The surface code is in effect a concatenated code with logical qubits encoded in corner twist Majorana fermions.

As noted in Sec. II A, Dirac fermions can be mapped onto pairs of Majorana fermions. Because twist defects act as logical Majorana fermions, one can remove one layer of abstraction, replacing both the Majorana cycle code (Sec. II E) and the Jordan-Wigner transformation (Sec. II B) with the mapping in Eq. (2). This creates the simplified simulation architecture stack in Fig. 8(b).

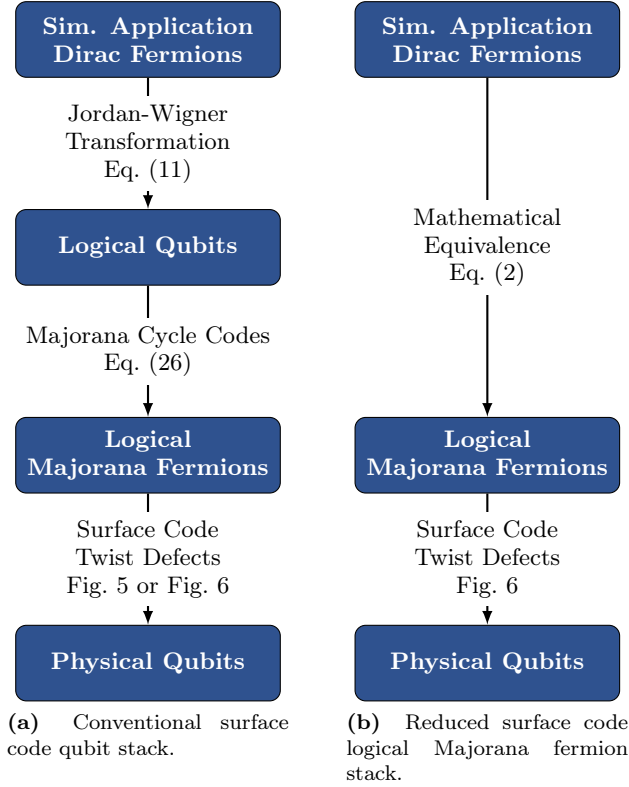


FIG. 8: The removal of an abstraction layer from the architecture stack used in error-corrected simulation applications.

Using this architecture, one can obtain scheduling and parallelization improvements to fermionic simulation algorithms by mapping local fermionic operations onto local logical fermionic operations, rather than onto highly nonlocal Jordan-Wigner strings on logical qubits, as depicted in Fig. 9.

Obtaining these improvements typically also involves some understanding of the system being simulated. For example, in Sec. IIIB, to fully exploit the square-lattice geometry of the fermionic 2D Fermi-Hubbard model, we move the corner twists of multiple surface-code patches, encoded as described in Sec. IIF, into interior twist defects arrayed in a 2D square lattice inside a single surface-code patch, as described in Sec. IIG. This allows us to reduce the asymptotic Trotter-Suzuki quantum circuit depth from $\mathcal{O}(\sqrt{N})$ in a Jordan-Wigner encoding as depicted in Fig. 9 to a depth of $\mathcal{O}(1)$. We describe this improvement in more detail in the upcoming Sec. IIIB, and we defer a description of how to interconvert between the different types of relevant surface codes to Appendix B.

Sometimes scheduling and parallelization improvements simply become more manifest in a direct mapping to logical fermions. For example, in Sec. IIIC, we describe how the SELECT operation in a qubitized approach to fermionic simulation (described in Sec. III), when applied to the 2D Fermi-Hubbard model, can be naturally optimized to reduce the T -count complexity of the algorithm by 20%, from $10N$ to $8N$, where N is the

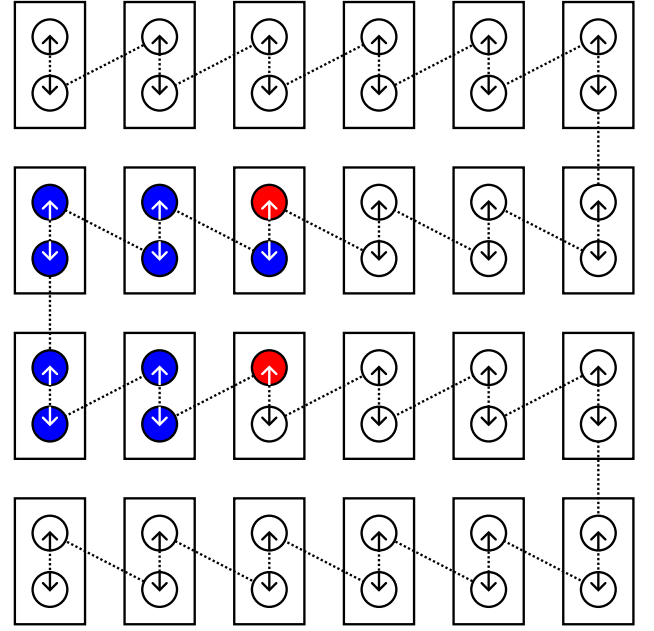


FIG. 9: A Jordan-Wigner “snaking string” for the Fermi-Hubbard model. It travels through two (Dirac) fermions per site, one spin-up and the other spin-down. An example nearest-neighbor hopping interaction $a_{p,\uparrow}^\dagger a_{q,\uparrow}$ between two sites gives rise to the highly non-local Pauli interaction $X_{p,\uparrow} \bar{Z} X_{q,\uparrow} + Y_{p,\uparrow} \bar{Z} Y_{q,\uparrow}$ depicted by the colored set of (Dirac) Fermi modes.

number of sites in the model. This optimization can even be applied (but less obviously so) in a more traditional Jordan-Wigner encoding. For this reason, we call this a *Majorana-inspired* speedup.

A. Logical measurement-based topological quantum computation

As noted in Sec. IIC, it is possible to realize universal quantum computation on Majorana fermionic quantum circuits solely through preparation and measurement operations on pairs and quads of Majorana fermions. Because of the relationship between Majorana fermions and Ising anyons, which are topological particles, this is essentially a representation of universal measurement-based topological quantum computation (MBTQC). In this section, we demonstrate how to realize MBTQC with the logical Majorana fermions represented by twist defects in surface codes, when the surface codes are interpreted as logical Majorana codes instead of logical qubit codes. While the majority of the fault-tolerant operations we describe follow from known constructions on logical qubits stored in surface codes, we are not aware of them being combined together to form a universal set of gates directly on the logical Majorana fermions.

In principle, one can construct a parsimonious version of universal logical MBTQC on surface codes solely us-

ing corner twists and lattice surgery operations on tetron and hexon patches. However, as we will see in Secs. III B and III C (and elaborated more in Appendix B), in the context of speedups to fault-tolerant fermionic quantum simulation algorithms, it is valuable to allow the corner twists to be brought to the interior so that fermionic quantum simulations can be accelerated. These interior twists can then be braided around one another by sequences of internal surface-code deformations.

To realize logical MBTQC, as a first step, one must map even-weight logical Majorana operators onto the physical qubit operators that encode them. These operators are the targets of logical state preparations and measurements. Again, although a parsimonious construction only requires logical Majorana operators of weight two and four (quadratic and quartic Majorana operators) as described in Sec. II C, we will show how to represent any even-weight operator, which opens up the possibility of further computational speedups in the context of fault-tolerant fermionic quantum simulation.

The representation of logical Majorana operators is straightforward: any string of physical Pauli operators on the qubits that encircles an even number of twists encodes the even-weight logical Majorana operator supported on those twists. Furthermore, the product of all of the logical Majorana operators on a surface-code patch is in the stabilizer group of the code, because it is just a representation of the conservation of total (logical) fermionic parity. If all corner twists are brought to the interior, a Pauli string that encircles them all can be pulled to the boundary and made to disappear, because there is nowhere for the string to “condense” on the boundary. This indicates that any surface-code patch holding only two Majorana fermions stores no information, and any surface-code patch containing only four Majorana fermions forces those fermions into a tetron code, or one that can be deformed into one by moving the twists to the corners; that is, tetron codes encode exactly a single logical qubit. Examples of quadratic and global Majorana operators are depicted in Fig. 10.

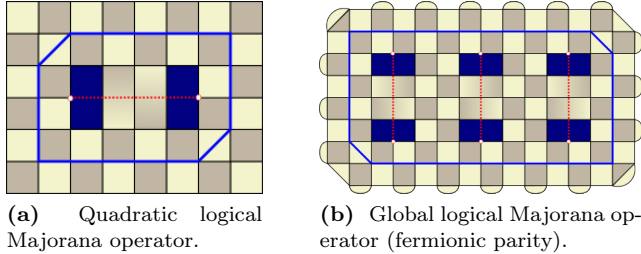


FIG. 10: (Color online.) Logical Majorana fermion operators encoded as physical qubit Pauli strings.

One of the key differences between universal quantum computation on logical qubits and logical Majorana fermions represented by surface-code patches is that there exist even-weight logical Majorana operators

that span multiple patches which have no representation in terms of logical-qubit operators. For example, a quadratic Majorana operator in which one twist is on one patch and one twist is on another has no meaning in terms of logical-qubit operators. That said, representing that operator even for logical Majorana fermions is problematic—two isolated surface code patches have no reason to be in a state of total fermionic parity conservation between them. To represent this operator, one must first deform the two patches so that they become a single patch. Only then can the two logical Majorana fermions “sense” one another. We describe how to do this code deformation in detail in Appendix B.

Once all twists are on the same patch, the quadratic logical Majorana operators and the individual logical qubit operators fall into one-to-one correspondence. In fact, more generally, all even-weight logical Majorana operators correspond to logical qubit operators that act on one or more logical qubits. Hence, fault-tolerant operations for realizing measurements and preparations of these operators, as described in Sec. II G, can be used to realize these operations fault-tolerantly. Although the operations described there acted on just one or two logical qubits at a time, they generalize straightforwardly to multi-qubit operations. For example, one can braid a puncture around a collection of pairs of interior twists to measure their joint Majorana operator fault-tolerantly. Or one can perform multi-logical-qubit lattice surgery with auxiliary patches to measure an even collection of corner twists. In essence, fault-tolerant MBTQC is automatically inherited from fault-tolerant logical-qubit computation on surface codes, once all the twists are moved to a single patch.

B. Trotterized Fermi-Hubbard model simulation exemplar

Consider a Trotter-Suzuki decomposition of the 2D Fermi-Hubbard model Hamiltonian on N sites, as represented in Eq. (38). As noted in Sec. II H, to perform this decomposition, one expresses the Hamiltonian as a sum of Trotter-layer Hamiltonians, where each such Trotter-layer Hamiltonian is a sum of commuting terms that do not necessarily commute with the terms in other layers.

In the Jordan-Wigner picture, the qubit Hamiltonian that we seek to Trotterize, following Babbush *et al.* [81], is the following:

$$H_{\text{HUB}} = -\frac{t}{2} \sum_{\langle p,q \rangle, \sigma} \left(X_{p,\sigma} \bar{Z} X_{q,\sigma} + Y_{p,\sigma} \bar{Z} Y_{q,\sigma} \right) + \frac{u}{4} \sum_p Z_{p,\uparrow} Z_{p,\downarrow} - \frac{u}{4} \sum_{p,\sigma} Z_{p,\sigma} + \frac{uN}{4} \mathbf{1}. \quad (39)$$

In this notation, X , Y , and Z are Pauli matrices acting on qubits at site p or q as indicated by the first index, and representing fermions with spin $\sigma \in \{\uparrow, \downarrow\}$ as indicated by the second index. The notation $X_{p,\sigma} \bar{Z} X_{q,\sigma}$ is a

shorthand for the nonlocal qubit operator

$$X_{p,\sigma} \vec{Z}_{q,\sigma} := X_{(p,\sigma)} Z_{(p,\sigma)+1} Z_{(p,\sigma)+2} \cdots Z_{(q,\sigma)-1} X_{(q,\sigma)}, \quad (40)$$

where $P_{(p,\sigma)+1}$ denotes the Pauli matrix P acting on the next combination of site and spin along the Jordan-Wigner string after $P(p,\sigma)$, as shown in Fig. 9.

While the final term in this Hamiltonian is proportional to the identity and therefore has no physical significance, it is usually kept so that the spectrum of this Hamiltonian matches that of the original Fermi-Hubbard model Hamiltonian.

This can be written as five Trotter layers. Every $Z_{p,\uparrow} Z_{p,\downarrow}$ and $Z_{p,\sigma}$ term commutes with every other such term, so all Z terms can be combined as a single layer. As for the $P_{p,\sigma} \vec{Z}_{q,\sigma}$ hopping terms, where $P \in \{X, Y\}$, they anticommute with any other hopping term with $\sigma = \sigma'$ and exactly one matching p or q . On a square lattice, each site has hopping terms in four directions, necessitating four different Trotter layers of hopping terms.

As discussed in Sec. II H, this does not necessarily allow a Trotter step to be implemented in depth 5, or even constant depth. As a standard architectural assumption, two commuting gates can only be run in parallel if they act on disjoint sets of qubits. For the the layer of on-site Z terms, this requires decomposition into two sub-layers; all the $Z_{p,\sigma}$ terms can be implemented simultaneously, but the $Z_{p,\uparrow} Z_{p,\downarrow}$ cannot be run in parallel with them. The Trotter-Suzuki simulation of the on-site terms, then, can still be run in $\mathcal{O}(1)$ depth.

Because nearest-neighbor fermions in a 2D lattice can be $\mathcal{O}(\sqrt{N})$ qubits away in a Jordan-Wigner encoding, as depicted in Fig. 9, the ability to parallelize the quantum simulation of the hopping terms is sharply limited. Each has support on $\mathcal{O}(\sqrt{N})$ qubits, and that bound is tight for at least one term on each site. By the disjointness requirement, one thus can exponentiate at most $\Theta(\sqrt{N})$ terms in parallel. Since there are $\Theta(N)$ hopping terms, each Trotter-Suzuki step has a minimum circuit depth (minimum number of Pauli product sub-layers) of $\Omega(\sqrt{N})$.

In contrast, in the Majorana fermion picture, because each Hamiltonian term is truly local, one can execute each Trotter-Suzuki step in $\mathcal{O}(1)$ depth. To see this, one first expands each Dirac fermion operator a with spin $\sigma \in \{\uparrow, \downarrow\}$ at 2D position $p = (x, y)$ into a pair of Majorana fermions c_- and c_+ , each of which is given the same spin value σ . After this, the Fermi-Hubbard model Hamiltonian can be expressed solely as a sum over individual sites as follows:

$$H_{\text{HUB}} = -\frac{t}{2} \sum_{(x,y,\sigma)} H_{\text{HUB}}^{(\text{int})}(x, y, \sigma) + \frac{u}{4} \sum_{(x,y)} H_{\text{HUB}}^{(\text{site})}(x, y) \quad (41)$$

$$H_{\text{HUB}}^{(\text{int})}(x, y, \sigma) = i c_{x,y,+, \sigma} c_{x+1,y,-, \sigma} + i c_{x+1,y,+, \sigma} c_{x,y,-, \sigma} + i c_{x,y,+, \sigma} c_{x,y+1,-, \sigma} + i c_{x,y+1,+, \sigma} c_{x,y,-, \sigma} \quad (42)$$

$$H_{\text{HUB}}^{(\text{site})}(x, y) = i c_{x,y,+, \uparrow} c_{x,y,-, \uparrow} + i c_{x,y,+, \downarrow} c_{x,y,-, \downarrow} - c_{x,y,+, \uparrow} c_{x,y,-, \uparrow} c_{x,y,+, \downarrow} c_{x,y,-, \downarrow} + \mathbb{1} \quad (43)$$

Each hopping term is local, whether in the horizontal x direction or vertical y direction, and is supported on exactly two Majorana fermions; there are $4N$ such terms, which can be implemented in four Majorana layers, plus another two layers for the on-site terms, which is very close (asymptotically identical) to the lower bound of five Trotter layers (the on-site terms commute with each other but anticommute with every hopping operator, and each Majorana fermion has four anticommuting hopping operators associated with it).

The stringlike logical operators corresponding to each of these terms in a logical Majorana surface code, in which each of the logical Majoranas is represented by an internal twist defect in the lattice, is depicted in Fig. 11. One challenge in realizing these stringlike logical operators is that they sometimes run very close to one another; in order to maintain a sufficient distance for fault-tolerance with the most compact packing of twists, first the odd-indexed terms for each layer can be evolved in parallel, then the even-indexed ones. Regardless, only a constant gate depth is required.

Unlike the speedups described in Sec. III C, this circuit depth reduction is actually reliant on access to Majorana fermions encoded as twist defects. This does not mean it is impossible to describe what is happening in the qubit picture: applying the Majorana cycle codes in Sec. II E allows the Majorana operators used to be mapped onto (in general, high-weight) Pauli operators with the same structure as Jordan-Wigner strings. However, those operators do not have the same disjoint support as the Majorana operators; and so the parallelization is only possible if the actual implementation of the exponentiated Hamiltonian terms happens at the Majorana level.

Furthermore, this construction utilized an encoding in which all twist defects are on a single patch; in Appendix B, we show that an implementation using a collection of tetron-encoded patches that interact via lattice surgery fails to achieve the same speedup. This suggests that, for at least some types of computational advantages, it is important to ensure that logical fermions are encoded in a way that reflects the layout of the fermions they are simulating.

C. Majorana-inspired qubitized Fermi-Hubbard model simulation exemplar

Simulating Hamiltonians with the qubitization algorithm requires the construction of a pair of oracles, PREPARE and SELECT, as described in Sec. III. For Hamil-

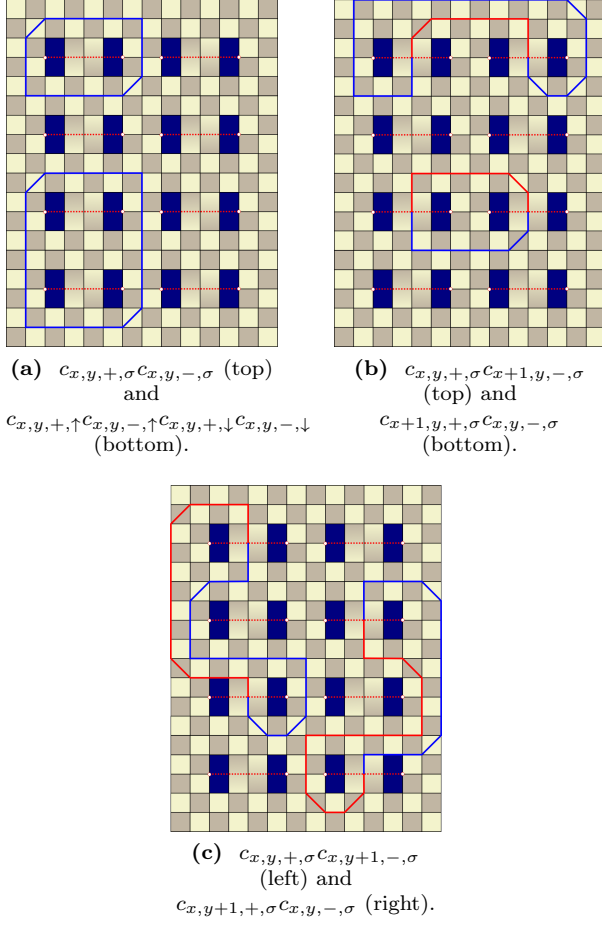


FIG. 11: The Hamiltonian terms of the Fermi-Hubbard model, drawn in solid lines as physical Pauli strings around logical Majorana twists, with X on sites in red and Z on sites in blue. Dark blue rectangles indicate weight-5 checks, and dashed lines mark missing qubits between pairs of twists.

tonians with many repeated coefficients, the costs of SELECT dominate. This is true, for example, for the Fermi-Hubbard model as studied, *e.g.*, in Ref. [81], for which PREPARE was implemented with T counts logarithmic in the system size N , whereas SELECT had a T count of $10N$ to leading-order.

By choosing our scheme for mapping Hamiltonian terms onto index bitstrings in a way that accounts for the limited connectivity of our Hamiltonians, more efficient implementations of SELECT become possible. For example, in the Fermi-Hubbard model, each Hamiltonian term is supported on, for each spin σ , either exactly one annihilation and one creation operator on spin-orbitals with spin σ ; or no fermionic operators with spin σ at all. As a result, we can uniquely specify a Hamiltonian term using four indices, each ranging over a quarter of the possible fermionic operators.

To see a reduction in T -count from these indexing scheme modifications, we will also need a variation on the

unary iteration circuits that have been previously used in implementing SELECT oracles. We refer to this variant of unary iteration, which introduces a parameter k to iterate over only $1/k$ of the qubits in a register while still applying Pauli strings across every qubit in the register, as “stride- k unary iteration,” and describe its implementation in Appendix C.

These circuits allow us to realize the benefits of the alternate indexing schemes; for example, in the Fermi-Hubbard model, we can reduce the T -count of each SELECT oracle call from $10N$ to $8N$ with the new indexing scheme and a stride-2 unary iteration circuit. We anticipate similar speedups can be realized by reindexing other Hamiltonians with similar structure.

We want to implement an block-encoding decomposition of the Fermi-Hubbard model Hamiltonian, Eq. (38). While Babbush *et al.* write this in terms of qubit operators via the Jordan-Wigner transformation as in Eq. (39), we will first choose to write it in terms of Majorana operators as

$$\sum_{\sigma} H_{\text{HUB}}^{(\text{int})}(x, y, \sigma) = i c_{p,+, \uparrow} \mathbb{1}_{+, \downarrow} c_{q,-, \uparrow} \mathbb{1}_{-, \downarrow} + i \mathbb{1}_{+, \uparrow} c_{p,+, \downarrow} \mathbb{1}_{-, \uparrow} c_{q,-, \downarrow} + i c_{q,+, \uparrow} \mathbb{1}_{+, \downarrow} c_{p,-, \uparrow} \mathbb{1}_{-, \downarrow} + i \mathbb{1}_{+, \uparrow} c_{q,+, \downarrow} \mathbb{1}_{-, \uparrow} c_{p,-, \downarrow} \quad (44)$$

$$\sum_{\sigma} H_{\text{HUB}}^{(\text{site})}(x, y) = i c_{p,+, \uparrow} \mathbb{1}_{+, \downarrow} c_{p,-, \uparrow} \mathbb{1}_{-, \downarrow} + i \mathbb{1}_{+, \uparrow} c_{p,+, \downarrow} \mathbb{1}_{-, \uparrow} c_{p,-, \downarrow} - c_{p,+, \uparrow} c_{p,+, \downarrow} c_{p,-, \uparrow} c_{p,-, \downarrow} + \mathbb{1}, \quad (45)$$

which differs from Eq. (41) in Sec. IIIB only in that we have explicitly included $\mathbb{1}_{\pm, \sigma}$ to draw attention to the fact that each term has the same form. In the Jordan-Wigner picture, these terms took the forms ZZ , Z , $X\bar{Z}X$, and $Y\bar{Z}Y$; while these do not initially appear to share a similar structure, the Majorana notation reveals that all four take the form $c_{j,+, \uparrow} c_{k,+, \downarrow} c_{l,-, \uparrow} c_{m,-, \downarrow}$. In other words, no term is supported on two of the same type (spin up or down, $+$ or $-$ Majorana) of Majorana operator on different sites; each is a product of up to one of each of the four.

In order to obtain our speedup, we are going to choose to label our terms with indices that correspond to this structure; in particular, we are going to label them with four (x, y) site coordinates j , k , l , and m , each corresponding to one of the four Majorana operators on that site.

In fact, while the Majorana paradigm made the possibility for this index scheme clear, we can apply the usual Jordan-Wigner encoding after re-indexing; the speedup itself is in no way dependent on the logical Majorana fermion implementation, so we call it a “Majorana-inspired” speedup. We write each Jordan-Wigner string a product of up to one of each of the four types of fermionic operators $\bar{Z}X_{p, \uparrow}$, $\bar{Z}X_{p, \downarrow}$, $\bar{Z}Y_{p, \uparrow}$, and $\bar{Z}Y_{p, \downarrow}$, as follows (for

$p < q$):

$$X_{p,\uparrow} \vec{Z} X_{q,\uparrow} = (\vec{Z} X_{q,\uparrow}) (\vec{Z} Y_{p,\uparrow}) \quad (46)$$

$$X_{p,\downarrow} \vec{Z} X_{q,\downarrow} = (\vec{Z} X_{q,\downarrow}) (\vec{Z} Y_{p,\downarrow}) \quad (47)$$

$$Y_{p,\uparrow} \vec{Z} Y_{q,\uparrow} = (\vec{Z} X_{p,\uparrow}) (\vec{Z} Y_{q,\uparrow}) \quad (48)$$

$$Y_{p,\downarrow} \vec{Z} Y_{q,\downarrow} = (\vec{Z} X_{p,\downarrow}) (\vec{Z} Y_{q,\downarrow}) \quad (49)$$

$$Z_{p,\uparrow} = (\vec{Z} X_{p,\uparrow}) (\vec{Z} Y_{p,\uparrow}) \quad (50)$$

$$Z_{p,\downarrow} = (\vec{Z} X_{p,\downarrow}) (\vec{Z} Y_{p,\downarrow}) \quad (51)$$

$$Z_{p,\uparrow} Z_{p,\downarrow} = (\vec{Z} X_{p,\uparrow}) (\vec{Z} Y_{p,\uparrow}) (\vec{Z} X_{p,\downarrow}) (\vec{Z} Y_{p,\downarrow}) \quad (52)$$

Factored in this way, the hidden common structure of the terms is clarified just as it was in the Majorana perspective.

If one of the four types of fermionic operator is not included in a particular term, we will have a special index-value for that, denoted here by \emptyset . Because of this, we will not need dedicated input wires to SELECT (the U and V in Babbush *et al.*) to denote whether we are considering a quadratic or quartic Majorana operator term; a quadratic term will have two \emptyset indices, and a quartic term will have none.

$$\begin{aligned} \text{PREPARE}_{\text{HUB}} |0\rangle^{\otimes 4+8 \lceil \log \sqrt{\frac{N}{2}+1} \rceil} &= \sum_{x=0}^{M-1} \sum_{y=0}^{M-1} \sqrt{\frac{t}{2\lambda}} \begin{bmatrix} |j_x j_y k_{x+1} k_y l_{\emptyset} m_{\emptyset}\rangle + |j_{x+1} j_y k_x k_y l_{\emptyset} m_{\emptyset}\rangle \\ + |j_x j_y k_x k_{y+1} l_{\emptyset} m_{\emptyset}\rangle + |j_x j_{y+1} k_x k_y l_{\emptyset} m_{\emptyset}\rangle \\ + |j_{\emptyset} k_{\emptyset} l_x l_y m_{x+1} m_y\rangle + |j_{\emptyset} k_{\emptyset} l_{x+1} l_y m_x m_y\rangle \\ + |j_{\emptyset} k_{\emptyset} l_x l_y m_x m_{y+1}\rangle + |j_{\emptyset} k_{\emptyset} l_x l_{y+1} m_x m_y\rangle \end{bmatrix} \\ &+ \sum_{x=0}^{M-1} \sum_{y=0}^{M-1} \sqrt{\frac{u}{8\lambda}} |j_x j_y k_x k_y l_x l_y m_x m_y\rangle \\ &+ \sum_{x=0}^{M-1} \sum_{y=0}^{M-1} \sqrt{\frac{u}{4\lambda}} [|j_x j_y k_x k_y l_{\emptyset} m_{\emptyset}\rangle + |j_{\emptyset} k_{\emptyset} l_x l_y m_x m_y\rangle] \end{aligned} \quad (53)$$

We use five auxiliary qubits to prepare this state. The first two flag whether we are constructing an $X\vec{Z}X/Y\vec{Z}Y$ term, a ZZ term, or a Z term, in the same manner as Babbush *et al.*'s U and V , except that we will not need to

pass them to SELECT. The next three determine which of the eight possible $X\vec{Z}X/Y\vec{Z}Y$ terms, or which of the two possible Z terms, we construct, by controlling how the various indices are SWAPPED around between registers.

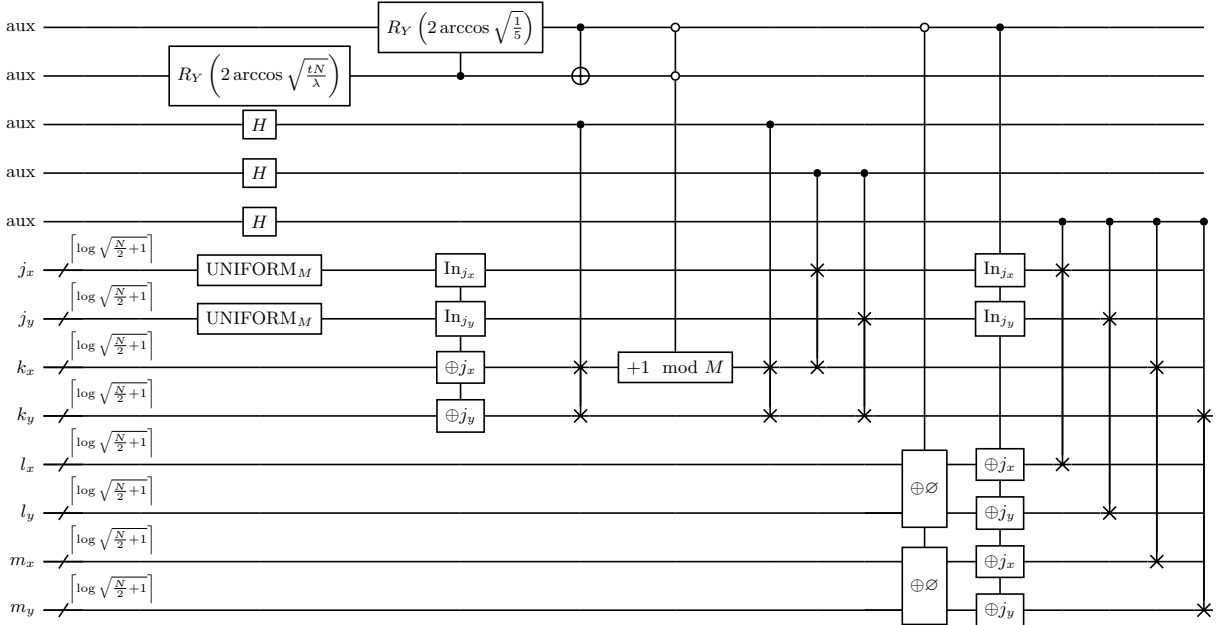


FIG. 12: The qubitized PREPARE oracle circuit.

Once we have prepared the correct index state, our SELECT operator just applies precisely the Jordan-Wigner-transformed Majorana operators specified by the index, using the stride- k unary iteration we described in Appendix C. Specifically, we will use the $k = 2$ version of the construction to iterate over only every other lattice

site—that is, either only the spin-up or only the spin-down sites—while still applying a Jordan-Wigner string operator on every lattice site, and will do so at only the T -cost of iterating over every other lattice site (that is, approximately half the T -cost of iterating over every lattice site).

$$\text{SELECT}_{\text{HUB}} |jklm\rangle |\psi\rangle = |jklm\rangle \otimes \left\{ \begin{array}{l} \mathbb{1} \\ \bar{Z}X_{j,\uparrow} \end{array} \right\} \left\{ \begin{array}{l} \mathbb{1} \\ \bar{Z}Y_{k,\uparrow} \end{array} \right\} \left\{ \begin{array}{l} \mathbb{1} \\ \bar{Z}X_{l,\downarrow} \end{array} \right\} \left\{ \begin{array}{l} \mathbb{1} \\ \bar{Z}Y_{m,\downarrow} \end{array} \right\} |\psi\rangle \quad (54)$$

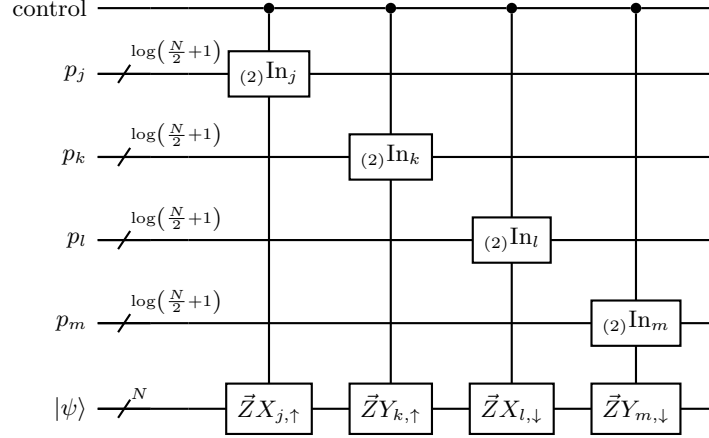


FIG. 13: The qubitized SELECT oracle circuit.

Each of the four unary iterations above iterates over $\frac{N}{2} + 1$ indices, and thus has a T -count of $2N$. In total, this means our SELECT implementation has a T -count of $8N + \mathcal{O}(\log N)$, compared to Babbush *et al.*'s $10N + \mathcal{O}(\log N)$.

IV. CONCLUSION

Inspired by Feynman's call to simulate quantum mechanics with quantum computers to eliminate the overhead in quantum-to-classical mappings [1], we have shown how to simulate fermions with error-corrected logical Majorana fermions in a way that eliminates the overhead in fermion-to-qubit mappings. We did so by processing the logical Majorana fermions stored as twist defects in surface code patches. We rely on known constructions on surface codes to implement the required operations for this processing, most of which have not been previously applied to the target of logical Majorana fermionic computation, but to the processing of logical qubits in Majorana cycle codes. We expect that these constructions will apply to topological codes more broadly than just the surface code, including those defined generally by rotation systems [48] and those defined dynamically, such as the honeycomb code [85, 86].

We demonstrate the value of the ability to manipu-

late logical Majorana fermions directly in a fault-tolerant setting for optimizing quantum simulation algorithms in the exemplar system of a 2D Fermi-Hubbard model. The improvements in this exemplar suggest that similar optimizations may be possible in other quantum simulation algorithms. In particular, removing elaborate nonlocal sequences of CNOT gates used to facilitate operations in the Jordan-Wigner mapping of qubits to fermions, such as those described in Refs. [81, 87–89], may lead to opportunities for parallel execution and scheduling optimizations.

Furthermore, we show the value of the logical fermionic data type as a conceptual tool to aid in quantum software development. By working in the abstraction of fermionic computation, we are able to obtain a T -count reduction for block encoding oracles in the same exemplar system, which is applicable even in non-fermionic architectures. We expect this approach to be a useful aid to algorithm developers examining other target applications as well.

Developing optimizing compilers that exploit the availability of native (Majorana) fermionic operations is an interesting avenue for further research. We look forward to seeing how the broad array of fermionic quantum simulation applications will be able to exploit the elimination of fermion-to-qubit mappings that we describe here.

As shown in Ref. [28], one can realize a rich panoply of anyons as twist defects in topological codes, even

beyond the simple Majorana fermions we have considered. This suggests that our approach is extendable in a way that facilitates low-overhead fault-tolerant anyonic simulation generally, using these logical anyons in the measurement-based topological quantum computing paradigm. For example, the Fradkin-Kadanoff transformation for parafermions that generalizes the Jordan-Wigner transformation for fermions might be able to be eliminated to facilitate less resource intensive studies of parafermions with quantum computers [90, 91]. Simulations of anyonic physics might even help to develop technology based on actual anyonic excitations in material systems [92].

While our approach may facilitate simulation studies of anyonic physics, including of Majorana fermions themselves, the fact that our constructions allow one to manipulate arbitrarily reliable “synthetic” logical Majorana fermions directly suggests that our approach could be an alternative to manipulating Majorana fermions realized as quasiparticle excitations in condensed matter systems for the purposes of reliable quantum computation. Much of the effort developed for how to manipulate Majorana fermions for the purposes of quantum computation, for example protocols for “topological quantum compiling,” [93] can be mapped to the logical Majorana fermion setting without any modifications. That said, the quest to realize physical Majorana fermions is still very important for fundamental physics and could be enabling for some quantum technologies.

It is worth noting that tailoring quantum error correcting codes for explicit use in fermionic quantum simulation algorithms is not a new idea; for example, see Refs. [11, 17–20]. However, all previous constructions of which we are aware either used *ad hoc* codes or only worked at fixed code distances which did not facilitate arbitrarily reliable quantum simulations. By basing our approach on surface codes, which have been studied extensively, our constructions will work at arbitrary code distances and could be realized by technologies built around

surface codes.

Acknowledgments

This paper benefited from helpful conversations from many people, including (in alphabetical order) Andrew Baczewski, Benjamin Brown, Riley Chien, Anand Ganti, Markus Kesselring, Daniel Litinski, Jesse Lutz, Setso Metodi, Stefan Seritan, Jaimie Stephens, James Whitfield, and Yijia Xu. We would like to thank the following people for their helpful feedback on an early draft of this paper: Andrew Baczewski, Lucas Kocia, Kenny Rudinger, Stefan Seritan, and Wayne Witzel. Finally, we thank Daniel Litinski, for inspiring the color scheme we used to depict surface codes.

This material is based upon work supported by the U.S. Department of Energy, Office of Science, National Quantum Information Science Research Centers. Additional support is acknowledged from National Nuclear Security Administration’s Advanced Simulation and Computing Program, and the Laboratory Directed Research and Development program at Sandia National Laboratories.

Sandia National Laboratories is a multimission laboratory managed and operated by National Technology and Engineering Solutions of Sandia, LLC., a wholly owned subsidiary of Honeywell International, Inc., for the U.S. Department of Energy’s National Nuclear Security Administration under contract DE-NA-0003525.

This paper describes objective technical results and analysis. Any subjective views or opinions that might be expressed in the paper do not necessarily represent the views of the U.S. Department of Energy or the United States Government.

-
- [1] R. P. Feynman, *Simulating physics with computers*, Int. J. Theo. Phys. **21**, 467 (1982), doi:10.1007/BF02650179.
 - [2] S. Lloyd, *Universal quantum simulators*, Science **273**, 1073 (1996), doi:10.1126/science.273.5278.1073.
 - [3] I. M. Georgescu, S. Ashhab, and F. Nori, *Quantum simulation*, Rev. Mod. Phys. **86**, 153 (2014), doi:10.1103/RevModPhys.86.153, arXiv:1308.6253.
 - [4] A. Aspuru-Guzik, W. Van Dam, E. Farhi, F. Gaitan, T. Humble, S. Jordan, A. J. Landahl, P. Love, R. Lucas, J. Preskill, et al., *ASCR Workshop on Quantum Computing for Science* (2015), doi:10.2172/1194404, URL <https://www.osti.gov/biblio/1194404>.
 - [5] E. Farhi, S. Jordan, P. Hayden, M. Lukin, J. Maldacena, J. Preskill, P. Shor, J. Taylor, and C. Williams, *Grand Challenges at the Interface of Quantum Information Science, Particle Physics, and Computing* (2015), URL https://science.osti.gov/-/media/hep/pdf/files/Banner-PDFs/QIS_Study_Group_Report.pdf.
 - [6] J. E. Moore, A. Aspuru-Guzik, B. Bauer, S. Coppersmith, W. de Jong, T. Devereaux, M. Fernandez-Serra, G. Galli, R. Harrison, P. Love, et al., *Basic Energy Sciences Roundtable: Opportunities for Quantum Computing in Chemical and Materials Sciences* (2017), doi:10.2172/1616253, URL <https://www.osti.gov/biblio/1616253>.
 - [7] J. Carlson, D. J. Dean, M. Hjorth-Jensen, D. Kaplan, J. Preskill, K. Roche, M. J. Savage, and M. Troyer, *Quantum Computing for Theoretical Nuclear Physics, A White Paper prepared for the U.S. Department of Energy, Office of Science, Office of Nuclear Physics* (2018), doi:10.2172/1631143, URL <https://www.osti.gov/biblio/1631143>.
 - [8] T. Schenkel, B. Dorland, A. Baczewski, M. Boshier, G. Collins, J. Dubois, A. Houck, T. Humble,

- N. Loureiro, C. Monroe, et al., *Fusion Energy Sciences Roundtable on Quantum Information Science* (2018), doi:10.2172/1615242, URL <https://www.osti.gov/biblio/1615242>.
- [9] B. Bauer, S. Bravyi, M. Motta, and G. K.-L. Chan, *Report on the NSF workshop on enabling quantum leap: Quantum algorithms for quantum chemistry and materials*, in *Report on a National Science Foundation Workshop, Alexandria, VA: January 21–24, 2019* (2019), arXiv:2001.03685, URL https://www.nsf.gov/mps/che/workshops/quantum_algorithms_for_chemistry_and_materials_report_01_21-24_2019.pdf.
- [10] Nuclear Science Advisory Committee (NSAC) Quantum Information Science (QIS) Subcommittee, *Nuclear Physics and Quantum Information Science* (2019), URL https://science.osti.gov/-/media/np/pdf/Reports/NSAC_QIS_Report.pdf.
- [11] Z. Jiang, A. Kalev, W. Mroczkiewicz, and H. Neven, *Optimal fermion-to-qubit mapping via ternary trees with applications to reduced quantum states learning*, *Quantum* **4**, 276 (2020), doi:10.22331/q-2020-06-04-276, arXiv:1910.10746.
- [12] P. Jordan and E. Wigner, *Über das Paulische Äquivalenzverbot*, *Z. Phys.* **47**, 631 (1928), doi:10.1007/BF01331938.
- [13] F. Verstraete and J. I. Cirac, *Mapping local Hamiltonians of fermions to local Hamiltonians of spins*, *J. Stat. Mech.: Theory and Experiment* **2005**, P09012 (2005), doi:10.1088/1742-5468/2005/09/P09012, arXiv:cond-mat/0508353.
- [14] S. Bravyi and A. Kitaev, *Fermionic quantum computation*, *Ann. Phys.* **298**, 210 (2002), doi:10.1006/aphy.2002.6254, arXiv:quant-ph/0003137.
- [15] J. T. Seeley, M. J. Richard, and P. J. Love, *The Bravyi-Kitaev transformation for quantum computation of electronic structure*, *J. Chem. Phys.* **137**, 224109 (2012), doi:10.1063/1.4768229, arXiv:1208.5986.
- [16] V. c. v. Havlíček, M. Troyer, and J. D. Whitfield, *Operator locality in the quantum simulation of fermionic models*, *Phys. Rev. A* **95**, 032332 (2017), doi:10.1103/PhysRevA.95.032332, arXiv:1701.07072.
- [17] Z. Jiang, J. McClean, R. Babbush, and H. Neven, *Majorana loop stabilizer codes for error correction of fermionic quantum simulations*, **12**, 064041 (2019), doi:10.1103/PhysRevApplied.12.064041, arXiv:1812.08190.
- [18] M. Steudtner and S. Wehner, *Quantum codes for quantum simulation of fermions on a square lattice of qubits*, *Phys. Rev. A* **99**, 022308 (2019), doi:10.1103/PhysRevA.99.022308, arXiv:1810.02681.
- [19] K. Setia, S. Bravyi, A. Mezzacapo, and J. D. Whitfield, *Superfast encodings for fermionic quantum simulation*, *Phys. Rev. Research* **1**, 033033 (2019), doi:10.1103/PhysRevResearch.1.033033, arXiv:1810.05274.
- [20] C. Derby and J. Klassen, *A compact fermion to qubit mapping*, **104**, 035118 (2020), doi:10.1103/PhysRevB.104.035118, arXiv:2003.06939.
- [21] W. Kirby, B. Fuller, C. Hadfield, and A. Mezzacapo, *Second-quantized fermionic Hamiltonians for quantum simulation with polylogarithmic qubit and gate complexity* (2021), arXiv:2109.14465.
- [22] E. Majorana, *Teoria simmetrica dell elettrone e del positrone. (Italian) [Symmetrical theory of the electron and the positron]*, *Il Nuovo Cimento* (8) **14**, 171 (1937), doi:10.1007/BF02961314.
- [23] M. Aghaee, A. Akkala, Z. Alam, R. Ali, A. A. Ramirez, M. Andrzejczuk, A. E. Antipov, P. Aseev, M. Astafev, B. Bauer, et al., *Inas-al hybrid devices passing the topological gap protocol* (2022), arXiv:2207.02472.
- [24] S. B. Bravyi and A. Y. Kitaev, *Quantum codes on a lattice with boundary* (1998), arXiv:quant-ph/9811052.
- [25] E. Dennis, A. Kitaev, A. Landahl, and J. Preskill, *Topological quantum memory*, *J. Math. Phys.* **43**, 4452 (2002), doi:10.1063/1.1499754, arXiv:quant-ph/0110143.
- [26] H. Bombin, *Topological order with a twist: Ising anyons from an Abelian model*, *Phys. Rev. Lett.* **105**, 030403 (2010), doi:10.1103/PhysRevLett.105.030403, arXiv:1004.1838.
- [27] B. J. Brown, K. Laubscher, M. S. Kesselring, and J. R. Wootton, *Poking holes and cutting corners to achieve Clifford gates with the surface code*, *Phys. Rev. X* **7**, 021029 (2017), doi:10.1103/PhysRevX.7.021029, arXiv:1609.04673.
- [28] M. S. Kesselring, F. Pastawski, J. Eisert, and B. J. Brown, *The boundaries and twist defects of the color code and their applications to topological quantum computation*, *Quantum* **2**, 101 (2018), doi:10.22331/q-2018-10-19-101, arXiv:1806.02820.
- [29] J. Bardeen, L. N. Cooper, and J. R. Schrieffer, *Microscopic theory of superconductivity*, *Phys. Rev.* **106**, 162 (1957), doi:10.1103/PhysRev.106.162.
- [30] J. Bardeen, L. N. Cooper, and J. R. Schrieffer, *Theory of superconductivity*, *Phys. Rev.* **108**, 1175 (1957), doi:10.1103/PhysRev.108.1175.
- [31] Y.-A. Chen and Y. Xu, *Equivalence between fermion-to-qubit mappings in two spatial dimensions* (2022), arXiv:2201.05153.
- [32] O. O'Brien and S. Strelchuk, *Ultrafast hybrid fermion-to-qubit mapping* (2022), arXiv:2211.16389.
- [33] H. Nishimura and M. Ozawa, *Computational complexity of uniform quantum circuit families and quantum Turing machines*, **276**, 147 (2002), doi:10.1016/S0304-3975(01)00111-6, arXiv:quant-ph/9906095.
- [34] Y. Li, *Fault-tolerant fermionic quantum computation based on color code*, *Phys. Rev. A* **98**, 012336 (2018), doi:10.1103/PhysRevA.98.012336, arXiv:1709.06245.
- [35] Z. Wang, *Topological quantum computation*, in *Topological Quantum Computation* (AMS, 2010), no. 112 in CBMW Regional Conference Series in Mathematics, p. 115.
- [36] J. K. Pachos, *Introduction to Topological Quantum Computation* (Cambridge University Press, 2012).
- [37] J. von Neumann, *Mathematical Foundations of Quantum Mechanics*, vol. 2 of *Investigations in physics* (Princeton University Press, Princeton, NJ, 1932 (Reprinted in paperback, 1955.)).
- [38] H. Zheng, A. Dua, and L. Jiang, *Measurement-only topological quantum computation without forced measurements*, *New J. Phys.* **18**, 123027 (2016), doi:10.1088/1367-2630/aa50bb, arXiv:1607.07475.
- [39] C. Chamberland, P. Iyer, and D. Poulin, *Fault-tolerant quantum computing in the Pauli or Clifford frame with slow error diagnostics*, **2**, 43 (2018), doi:10.22331/q-2018-01-04-43, arXiv:1704.06662.

- [40] D. Litinski, *A game of surface codes: Large-scale quantum computing with lattice surgery*, Quantum **3**, 128 (2019), [doi:10.22331/q-2019-03-05-128](https://doi.org/10.22331/q-2019-03-05-128), [arXiv:1808.02892](https://arxiv.org/abs/1808.02892).
- [41] P. Bonderson, M. Freedman, and C. Nayak, *Measurement-only topological quantum computation*, Phys. Rev. Lett. **101**, 010501 (2008), [doi:10.1103/PhysRevLett.101.010501](https://doi.org/10.1103/PhysRevLett.101.010501), [arXiv:0802.0279](https://arxiv.org/abs/0802.0279).
- [42] M. Barkeshli and M. Freedman, *Modular transformations through sequences of topological charge projections*, Phys. Rev. B **94**, 165108 (2016), [doi:10.1103/PhysRevB.94.165108](https://doi.org/10.1103/PhysRevB.94.165108), [arXiv:1602.01093](https://arxiv.org/abs/1602.01093).
- [43] A. Tran, A. Bocharov, B. Bauer, and P. Bonderson, *Optimizing Clifford gate generation for measurement-only topological quantum computation with Majorana zero modes*, SciPost Phys. **8**, 091 (2020), [doi:10.21468/SciPostPhys.8.6.091](https://doi.org/10.21468/SciPostPhys.8.6.091), [arXiv:1909.03002](https://arxiv.org/abs/1909.03002).
- [44] S. Bartolucci, P. Birchall, H. Bombin, H. Cable, C. Dawson, M. Gimeno-Segovia, E. Johnston, K. Kieling, N. Nickerson, M. Pant, et al., *Fusion-based quantum computation* (2021), [arXiv:2101.09310](https://arxiv.org/abs/2101.09310).
- [45] S. Bravyi, B. Leemhuis, and B. M. Terhal, *Majorana fermion codes*, New J. Phys. **12**, 083039 (2010), [doi:10.1088/1367-2630/12/8/083039](https://doi.org/10.1088/1367-2630/12/8/083039), [arXiv:1004.3791](https://arxiv.org/abs/1004.3791).
- [46] D. Gottesman, *Stabilizer codes and quantum error correction*, Ph.D. thesis, Caltech (1997), [arXiv:quant-ph/9705052](https://arxiv.org/abs/quant-ph/9705052).
- [47] S. Vijay and L. Fu, *Quantum error correction for complex and Majorana fermion qubits* (2017), [arXiv:1703.0459](https://arxiv.org/abs/1703.0459).
- [48] R. Sarkar and T. J. Yoder, *A graph-based formalism for surface codes and twists* (2021), [arXiv:2101.09349](https://arxiv.org/abs/2101.09349).
- [49] D. Litinski and F. von Oppen, *Quantum computing with Majorana fermion codes*, Phys. Rev. B **97**, 205404 (2018), [doi:10.1103/PhysRevB.97.205404](https://doi.org/10.1103/PhysRevB.97.205404), [arXiv:1801.08143](https://arxiv.org/abs/1801.08143).
- [50] S. Bravyi, *Universal quantum computation with the $\nu=5/2$ fractional quantum Hall state*, Phys. Rev. A **73**, 042313 (2006), [doi:10.1103/PhysRevA.73.042313](https://doi.org/10.1103/PhysRevA.73.042313), [arXiv:quant-ph/0511178](https://arxiv.org/abs/quant-ph/0511178).
- [51] M. Hastings, T. Karzig, P. Bonderson, M. Freedman, R. Lutchyn, and C. Nayak, *Quantum computing methods and devices for Majorana tetron qubits* (pending), URL <https://patents.google.com/patent/US20180052806A1/en>.
- [52] In an earlier preprint of this paper, we instead utilized the less efficient multiple-tetron encoding, [arXiv:2110.10280](https://arxiv.org/abs/2110.10280).
- [53] A. Y. Kitaev, *Quantum error correction with imperfect gates*, in *Proceedings of the Third International Conference on Quantum Communication, Computing and Measurement*, edited by O. Hirota, A. S. Holevo, and C. M. Caves (Plenum Press, New York, 1997), p. 181.
- [54] A. Y. Kitaev, *Fault-tolerant quantum computation by anyons*, Ann. Phys. **303**, 2 (2003), [doi:10.1016/S0003-4916\(02\)00018-0](https://doi.org/10.1016/S0003-4916(02)00018-0), [arXiv:quant-ph/9707021](https://arxiv.org/abs/quant-ph/9707021).
- [55] A. Y. Kitaev, *Quantum computations: Algorithms and error correction*, Russian Math. Surveys **52**, 1191 (1997), [doi:10.1070/RM1997v052n06ABEH002155](https://doi.org/10.1070/RM1997v052n06ABEH002155).
- [56] M. H. Freedman and D. A. Meyer, *Projective plane and planar quantum codes*, Found. Comput. Math. **1**, 325 (2001), [doi:10.1007/s102080010013](https://doi.org/10.1007/s102080010013), [arXiv:quant-ph/9810055](https://arxiv.org/abs/quant-ph/9810055).
- [57] H. Bombin and M. A. Martin-Delgado, *Topological quantum error correction with optimal encoding rate*, Phys. Rev. A **73**, 062303 (2006), [doi:10.1103/PhysRevA.73.062303](https://doi.org/10.1103/PhysRevA.73.062303), [arXiv:quant-ph/0602063](https://arxiv.org/abs/quant-ph/0602063).
- [58] H. Bombin and M. A. Martin-Delgado, *Optimal resources for topological two-dimensional stabilizer codes: Comparative study*, Phys. Rev. A **76**, 012305 (2007), [doi:10.1103/PhysRevA.76.012305](https://doi.org/10.1103/PhysRevA.76.012305), [arXiv:quant-ph/0703272](https://arxiv.org/abs/quant-ph/0703272).
- [59] J. T. Anderson, *Homological stabilizer codes* (2011), [arXiv:1107.3502](https://arxiv.org/abs/1107.3502).
- [60] J. P. B. Ataides, D. K. Tuckett, S. D. Bartlett, S. T. Flammia, and B. J. Brown, *The XZZX surface code*, **12**, 2172 (2021), [doi:10.1038/s41467-021-22274-1](https://doi.org/10.1038/s41467-021-22274-1), [arXiv:2009.07851](https://arxiv.org/abs/2009.07851).
- [61] A. Kitaev and L. Kong, *Models for gapped boundaries and domain walls*, Commun. Math. Phys. **313**, 351 (2012), [doi:10.1007/s00220-012-1500-5](https://doi.org/10.1007/s00220-012-1500-5), [arXiv:1104.5047](https://arxiv.org/abs/1104.5047).
- [62] Y.-Z. You and X.-G. Wen, *Projective non-Abelian statistics of dislocation defects in a z_n rotor model*, Phys. Rev. B **86**, 161107(R) (2012), [doi:10.1103/PhysRevB.86.161107](https://doi.org/10.1103/PhysRevB.86.161107), [arXiv:1204.0113](https://arxiv.org/abs/1204.0113).
- [63] Y.-Z. You, C.-M. Jian, and X.-G. Wen, *Synthetic non-Abelian statistics by Abelian anyon condensation*, Phys. Rev. B **87**, 045106 (2013), pre-print has a different title., [doi:10.1103/PhysRevB.87.045106](https://doi.org/10.1103/PhysRevB.87.045106), [arXiv:1208.4109](https://arxiv.org/abs/1208.4109).
- [64] T. J. Yoder and I. H. Kim, *The surface code with a twist*, Quantum **1**, 2 (2017), [doi:10.22331/q-2017-04-25-2](https://doi.org/10.22331/q-2017-04-25-2), [arXiv:1612.04795](https://arxiv.org/abs/1612.04795).
- [65] B. J. Brown and S. Roberts, *Universal fault-tolerant measurement-based quantum computation*, Phys. Rev. Research **2**, 033305 (2020), [doi:10.1103/PhysRevResearch.2.033305](https://doi.org/10.1103/PhysRevResearch.2.033305), [arXiv:1811.11780](https://arxiv.org/abs/1811.11780).
- [66] A. Lavasani and M. Barkeshli, *Low overhead Clifford gates from joint measurements in surface, color, and hyperbolic codes*, Phys. Rev. A **98**, 052319 (2018), [doi:10.1103/PhysRevA.98.052319](https://doi.org/10.1103/PhysRevA.98.052319), [arXiv:1804.04144](https://arxiv.org/abs/1804.04144).
- [67] M. Barkeshli, P. Bonderson, M. Cheng, and Z. Wang, *Symmetry fractionalization, defects, and gauging of topological phases*, Phys. Rev. B **100**, 115147 (2019), [doi:10.1103/PhysRevB.100.115147](https://doi.org/10.1103/PhysRevB.100.115147), [arXiv:1410.4540](https://arxiv.org/abs/1410.4540).
- [68] G. Zhu, M. Hafezi, and M. Barkeshli, *Quantum origami: Transversal gates for quantum computation and measurement of topological order*, Phys. Rev. Research **2**, 013285 (2020), [doi:10.1103/PhysRevResearch.2.013285](https://doi.org/10.1103/PhysRevResearch.2.013285), [arXiv:1711.05752](https://arxiv.org/abs/1711.05752).
- [69] H. Bombin, C. Dawson, R. V. Mishmash, N. Nickerson, F. Pastawski, and S. Roberts, *Logical blocks for fault-tolerant topological quantum computation* (2021), [arXiv:2112.12160](https://arxiv.org/abs/2112.12160).
- [70] S. Vijay, T. H. Hsieh, and L. Fu, *Majorana fermion surface code for universal quantum computation*, Phys. Rev. X **5**, 041038 (2015), [doi:10.1103/PhysRevX.5.041038](https://doi.org/10.1103/PhysRevX.5.041038), [arXiv:1504.01724](https://arxiv.org/abs/1504.01724).
- [71] S. Vijay and L. Fu, *Physical implementation of a Majorana fermion surface code for fault-tolerant quantum computation*, Physica Scripta **T168**, 014002 (2016), [doi:10.1088/0031-8949/T168/1/014002](https://doi.org/10.1088/0031-8949/T168/1/014002), [arXiv:1509.08134](https://arxiv.org/abs/1509.08134).
- [72] D. Litinski and F. von Oppen, *Braiding by Majorana tracking and long-range CNOT gates with*

- color codes, *Phys. Rev. B* **96**, 205413 (2017), [doi:10.1103/PhysRevB.96.205413](#), [arXiv:1708.05012](#).
- [73] A. J. Landahl and C. Ryan-Anderson, *Quantum computing by color-code lattice surgery* (2014), [arXiv:1407.5103](#).
- [74] C. Horsman, A. G. Fowler, S. Devitt, and R. van Meter, *Surface code quantum computing by lattice surgery*, *New J. Phys.* **14**, 123011 (2012), [doi:10.1088/1367-2630/14/12/123011](#), [arXiv:1111.4022](#).
- [75] C. Cesare, A. J. Landahl, D. Bacon, S. T. Flammia, and A. Neels, *Adiabatic topological quantum computing* (2014), [arXiv:1406.2690](#).
- [76] S. Bravyi and A. Kitaev, *Universal quantum computation with ideal Clifford gates and noisy ancillas*, *Phys. Rev. A* **71**, 022316 (2005), [doi:10.1103/PhysRevA.71.022316](#), [arXiv:quant-ph/0403025](#).
- [77] H. Bombin, I. H. Kim, D. Litinski, N. Nickerson, M. Pant, F. Pastawski, S. Roberts, and T. Rudolph, *Interleaving: Modular architectures for fault-tolerant photonic quantum computing* (2021), [arXiv:2103.08612](#).
- [78] M. Suzuki, *Fractal decomposition of exponential operators with applications to many-body theories and monte carlo simulations*, *Physics Letters A* **146**, 319 (1990), ISSN 0375-9601, [doi:https://doi.org/10.1016/0375-9601\(90\)90962-N](#).
- [79] A. G. Fowler, M. Mariantoni, J. M. Martinis, and A. N. Cleland, *Surface codes: Towards practical large-scale quantum computation*, *Phys. Rev. A* **86**, 032324 (2012), [doi:10.1103/PhysRevA.86.032324](#), [arXiv:1208.0928](#).
- [80] G. H. Low and I. L. Chuang, *Hamiltonian simulation by qubitization*, *Quantum* **3**, 163 (2019), [doi:10.22331/q-2019-07-12-163](#), [arXiv:1610.06546](#).
- [81] R. Babbush, C. Gidney, D. W. Berry, N. Wiebe, J. McClean, A. Paler, A. Fowler, and H. Neven, *Encoding electronic spectra in quantum circuits with linear T complexity*, *Phys. Rev. X* **8**, 041015 (2018), [doi:10.1103/PhysRevX.8.041015](#), [arXiv:1805.03662](#).
- [82] J. Hubbard and B. H. Flowers, *Electron correlations in narrow energy bands*, *Proceedings of the Royal Society of London. Series A. Mathematical and Physical Sciences* **276**, 238 (1963), [doi:10.1098/rspa.1963.0204](#).
- [83] J. P. F. LeBlanc, A. E. Antipov, F. Becca, I. W. Bulik, G. K.-L. Chan, C.-M. Chung, Y. Deng, M. Ferrero, T. M. Henderson, C. A. Jiménez-Hoyos, et al. (Simons Collaboration on the Many-Electron Problem), *Solutions of the two-dimensional hubbard model: Benchmarks and results from a wide range of numerical algorithms*, *Phys. Rev. X* **5**, 041041 (2015), [doi:10.1103/PhysRevX.5.041041](#), [arXiv:1505.02290](#).
- [84] P.-L. Dallaire-Demers and F. K. Wilhelm, *Quantum gates and architecture for the quantum simulation of the fermi-hubbard model*, *Phys. Rev. A* **94**, 062304 (2016), [doi:10.1103/PhysRevA.94.062304](#), [arXiv:1606.00208](#).
- [85] M. B. Hastings and J. Haah, *Dynamically generated logical qubits* (2021), [arXiv:2107.02194](#).
- [86] C. Gidney, M. Newman, A. Fowler, and M. Broughton, *A fault-tolerant honeycomb memory* (2021), [arXiv:2108.10457](#).
- [87] V. von Burg, G. H. Low, T. Häner, D. S. Steiger, M. Reiher, M. Roetteler, and M. Troyer, *Quantum computing enhanced computational catalysis*, **3**, 033055 (2021), [doi:10.1103/physrevresearch.3.033055](#), [arXiv:2007.14460](#).
- [88] J. Lee, D. W. Berry, C. Gidney, W. J. Huggins, J. R. McClean, N. Wiebe, and R. Babbush, *Even more efficient quantum computations of chemistry through tensor hypercontraction*, **2**, 030305 (2021), [doi:10.1103/PRXQuantum.2.030305](#), [arXiv:2011.03494](#).
- [89] K. Wan, *Exponentially faster implementations of $Select(H)$ for fermionic Hamiltonians*, p. 380 (2021), [doi:10.22331/q-2021-01-12-380](#), [arXiv:2004.04170](#).
- [90] Z.-H. Liu, K. Sun, J. K. Pachos, M. Yang, Y. Meng, Y.-W. Liao, Q. Li, J.-F. Wang, Z.-Y. Luo, Y.-F. He, et al., *Topological contextuality and anyonic statistics of photonic-encoded parafermions*, *PRX Quantum* **2**, 030323 (2021), [doi:10.1103/PRXQuantum.2.030323](#), [arXiv:2011.05008](#).
- [91] E. Fradkin and L. P. Kadanoff, *Disorder variables and para-fermions in two-dimensional statistical mechanics*, *Nuc. Phys. B* **170**, 1 (1980), [doi:https://doi.org/10.1016/0550-3213\(80\)90472-1](#).
- [92] C. W. J. Beenakker, *Search for Majorana fermions in superconductors*, *Annu. Rev. Con. Mat. Phys.* **4**, 113 (2013), [doi:10.1146/annurev-conmatphys-030212-184337](#), [arXiv:1112.1950](#).
- [93] V. Kliuchnikov, A. Bocharov, and K. M. Svore, *Asymptotically optimal topological quantum compiling*, *Phys. Rev. Lett.* **112**, 140504 (2014), [doi:10.1103/PhysRevLett.112.140504](#), [arXiv:1310.4150](#).
- [94] C. Gidney and R. Babbush, *Performing unitary iteration and indexed operations*.

Appendix A: Unary iteration circuits

The block-encoding oracles for the Hubbard model in Ref. [81], as mentioned in Sec. II J, rely on the quantum algorithmic primitive of unary iteration [94]. Our block-encoding oracles in Sec. III C will use a modified version of that primitive, which we construct in Appendix C. We briefly describe here the standard version of unary iteration, for comparison.

In general, the unary iteration primitive implements the operation

$$|c\rangle |l\rangle |\psi\rangle \rightarrow |c\rangle |l\rangle \Lambda_c(\hat{A}_l) |\psi\rangle \quad (\text{A1})$$

for a collection of operations $\hat{A}_0 \dots \hat{A}_{L-1}$ with T -count $4L - 4$ plus any T -cost for implementing the A_l , where $\Lambda_c(U)$ denotes the controlled- U operation, controlled on the state of the qubit $|c\rangle$. The specific implementation used in the SELECT oracles of Ref. [81] specializes this to “ranged and indexed” operations

$$|c\rangle |l\rangle |\psi\rangle \rightarrow |c\rangle |l\rangle \Lambda_c \left(\bigotimes_{i=0}^{l-1} \hat{P}_i \otimes \hat{Q}_l \right) |\psi\rangle \quad (\text{A2})$$

where P_i and $Q_i \in X_i, Y_i, Z_i, I_i$ are Pauli operators acting on qubit i of the ψ register. This is done by the following circuit construction:

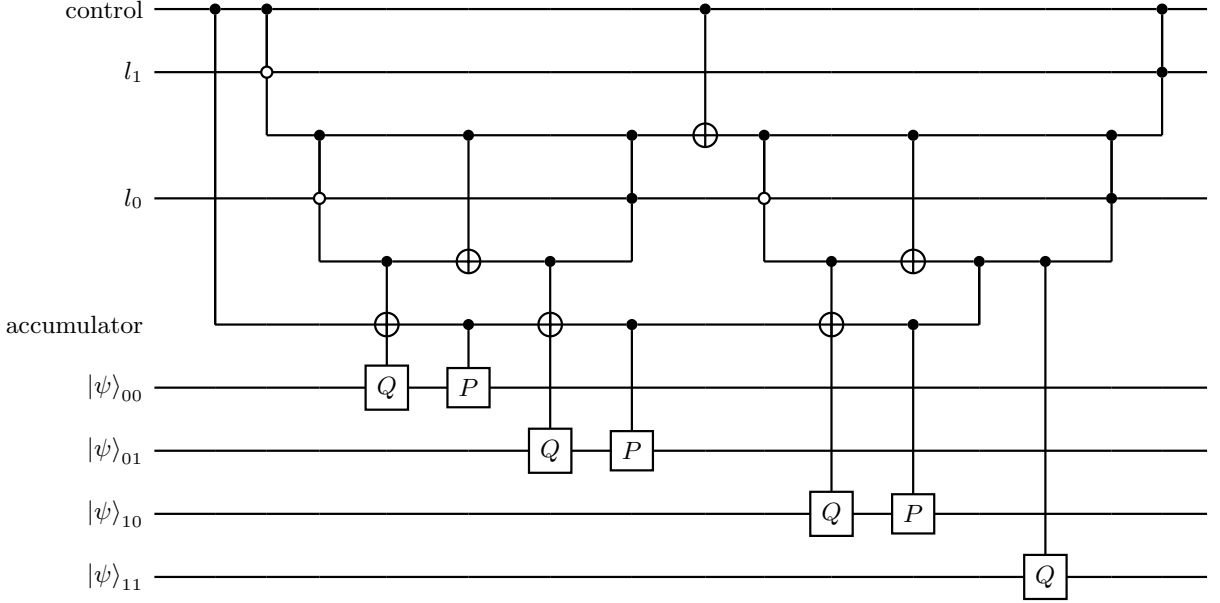


FIG. 14: A general ranged and indexed operator implemented using unary iteration.

As noted in Ref. [81], this construction can be transformed much as classical iterators can; in Appendix C we discuss a transformation of particular utility for our work.

Appendix B: Code deformation between the n -tetron and $(2n + 2)$ -on encodings

As we noted in Sec. III A, a quadratic logical Majorana fermion operator that spans two different tetron surface-code patches has no representation in terms of logical-qubit operators. In order for this operator to have meaning, even for logical Majorana fermions, the twists where they reside need to be brought onto the same surface-code patch so that they can “sense” one another through a global fermionic parity constraint (which is equal to the product of all the stabilizer generators of the collective patch). This is necessary, generically, for fault-tolerant fermionic quantum simulation algorithms that exploit logical Majorana fermions directly, because, generally, a fermionic Hamiltonian can include quadratic operators between any pair of logical Majorana fermions.

That said, one might wish to store logical Majorana fermions on tetron patches for ease of implementation; one might imagine that one could transform the information carriers between the $(2n + 2)$ -fermion Majorana cycle code and an array of n tetron codes on demand. Unfortunately, we will see that, while this is possible, it is sufficiently nonlocal and expensive as to obviate any locality-derived scheduling improvements one might have obtained.

Even if we are not intending to use our logical Ma-

jorana fermions to implement logical qubits, the operators described in Sec. II E for logical Pauli operators form a complete set of generators for the group of logical Majorana fermion operators available within the code (that is, excluding any that anti-commute with stabilizer-group elements—most notably the odd-weight operators—and treating each operator as its equivalence class under stabilizer-element multiplication). Specifically, the n -tetron code has the same stabilizer generators as are enforced by n four-logical-Majorana-fermion square patches, and the $(2n + 2)$ -logical-Majorana-fermion cycle code has the same stabilizer generators as the dislocation twist defect code. Accordingly, we can use the stabilizer formalism [46] to track the code deformations we perform.

Suppose we wish to deform from a cycle code with $2n + 2$ logical Majorana fermions on a single patch to a code with patches of four logical Majorana fermions each. We consider two different versions of this deformation. In the first, only defined when n is odd, we keep the fermion number constant, and split the large patch into $\frac{n+1}{2}$ tetron patches. However, adding $\frac{n-1}{2}$ additional stabilizer generators but keeping the number of information carriers constant will shrink our logical subspace, and we will lose information. Instead, we will need to add $2n - 2$ additional logical Majorana fermions, leaving us with a total of $4n$ logical Majorana fermions on n tetron patches. Thus, we will have added precisely half as many checks as logical Majorana fermions, and so the dimension of our logical subspace remains constant.

For ease of description, we use four additional auxiliary logical Majorana fermions during the deformation; they can be optimized away, but doing so makes the operation

less clear. Suppose we have a linear array of $2n + 2$ Majorana fermions $c_0 \dots c_{2n+1}$ on a single patch. Our logical operator generators are

$$L_k = \prod_{i=0}^k c_{2i} c_{2i+1} \quad (B1)$$

$$L'_k = c_{2k+1} c_{2k+2} \quad (B2)$$

for $0 \leq k < n$ as described above. Our only stabilizer generator is the product

$$S_G = \prod_{i=0}^{2n+1} c_i \quad (B3)$$

of all the logical Majorana operators (that is, global parity conservation).

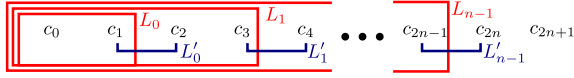


FIG. 15: (Color online.) The initial logical operators and stabilizer generator for the linear logical Majorana array.

To begin the deformation, introduce a second line of logical Majorana fermions $c_{2n+2} \dots c_{4n+3}$ prepared in the $+1$ eigenstate of a new set of stabilizer generators

$$S_k = c_{(2n+2)+2k} c_{(2n+2)+(2k+1)} \quad (B4)$$

$$S_F = \prod_{i=2n+2}^{4n+3} c_i. \quad (B5)$$

By multiplying by these stabilizer generators, we can rewrite our logical operator generators as

$$\begin{aligned} L_k &\rightarrow L_k \prod_{i=0}^k S_i \\ &= \prod_{i=0}^k c_{2i} c_{2i+1} c_{(2n+2)+2i} c_{(2n+2)+(2i+1)} \end{aligned} \quad (B6)$$

(with no change to the L'_k).

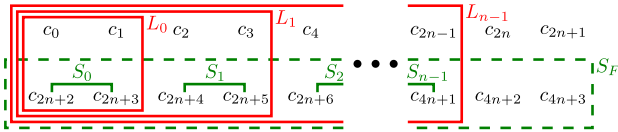


FIG. 16: (Color online.) The second line of logical Majorana fermions, new stabilizer generators, and extended logical operators produced.

We can then, one at a time from $k = n - 1$ to $k = 0$, replace each S_k with the anticommuting stabilizer generator

$$\tilde{S}_k = c_{2k+1} c_{2k+2} c_{(2n+2)+(2k+1)} c_{(2n+2)+(2k+2)}. \quad (B7)$$

Note that, if the replacements are done in descending order of k , the new stabilizer generator will commute with all of our other existing stabilizer and logical operators.

Next, take the stabilizer generator S_F and multiply it by the product of all the other stabilizer generators, rewriting it as

$$\begin{aligned} S_F &\rightarrow -S_F S_G \prod_{k=0}^{n-1} \tilde{S}_k \\ &= c_0 c_{2n+1} c_{2n+2} c_{4n+3}. \end{aligned} \quad (B8)$$

Take S_G and replace it with the anticommuting stabilizer generator

$$\tilde{S}_G = c_{2n+1} c_{4n+3}. \quad (B9)$$

As with our other replacements, this commutes with every stabilizer and logical operator generator except for the old S_G it replaces.

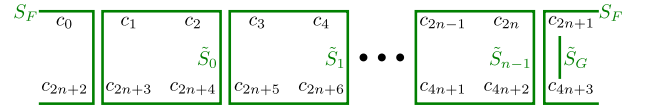


FIG. 17: (Color online.) The stabilizer generators after rewriting S_F and replacing S_k and S_G .

If we then multiply S_F by the new \tilde{S}_G , yielding

$$S_F \rightarrow S_F \tilde{S}_G = c_0 c_{2n+2}, \quad (B10)$$

we find that \tilde{S}_G is the *only* stabilizer generator supported on either c_{2n+1} or c_{4n+3} ; accordingly, we can measure those two logical Majorana fermions off, removing \tilde{S}_G entirely.

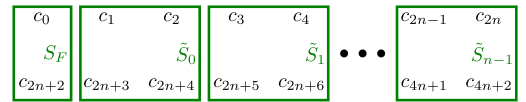


FIG. 18: (Color online.) The stabilizer generators after rewriting S_F again and measuring off c_{2n+1} and c_{4n+3} .

Finally, we can rewrite each L_k as the equivalent-up-to-stabilizer-group-multiplication

$$\begin{aligned} L_k &\rightarrow L_k S_F \prod_{i=0}^{k-1} \tilde{S}_i \\ &= c_{2k+1} c_{(2n+2)+(2k+1)}, \end{aligned} \quad (B11)$$

leaving S_F as the only stabilizer generator supported on c_0 and c_{2n+2} . We measure it off just as we did \tilde{S}_G , leaving us with the n tetron stabilizer generators \tilde{S}_k . Note that, as expected, each L_k still anticommutes with the corresponding L'_k , which has been preserved unchanged from our original code.

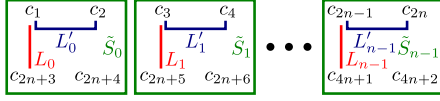


FIG. 19: (Color online.) The stabilizer generators in the final tetron code after the deformation is complete.

Thus, we have performed the desired code deformation, from $2n + 2$ logical Majorana fermions and one weight- $(2n + 2)$ stabilizer generator to $4n$ logical Majorana fermions with n weight-4 stabilizer generators, and all our logical information preserved. Of course, this whole process can be performed in reverse, exchanging preparations and measurements, to deform the code in the other direction. Furthermore, any logical Majorana fermionic operator that was even-weight (globally parity-preserving) on the original code is now even-weight on *each patch* of the new code (locally parity-preserving). Thus, any such operator could, if desired, be measured via *standard* (albeit potentially wildly nonlocal) lattice surgery operations.

But what did it cost us? Our code deformation interacts with every logical Majorana fermion, and indeed introduces a new weight- $(2n + 2)$ stabilizer generator. In other words, it is as nonlocal as a code deformation could possibly be; we should not find this surprising, because we needed to take the extremely nonlocal

$$L_{n-1} = \prod_{i=0}^{n-1} c_{2i} c_{2i+1} \quad (\text{B12})$$

to a completely local (weight-2) operator. If one was hoping, by using tetron surface-code patches instead of one giant patch, that logical Majorana operations would be more local, or easier to route, or some similar benefit over nonlocal logical Jordan-Wigner operations, such benefits disappear when accounting for the the cost of moving

between the many-tetron and one-giant-patch encoding.

Appendix C: Stride- k unary iteration circuits

While constructing the block-encoding circuits in Sec. III C, we discovered that we required a slightly different construction of the unary-iterated Majorana operators [94] than that used by Babbush *et al.* [81]. We refer to this construction as *stride* unary iteration by analogy to the stride parameter present in many classical programming languages' iteration constructs.

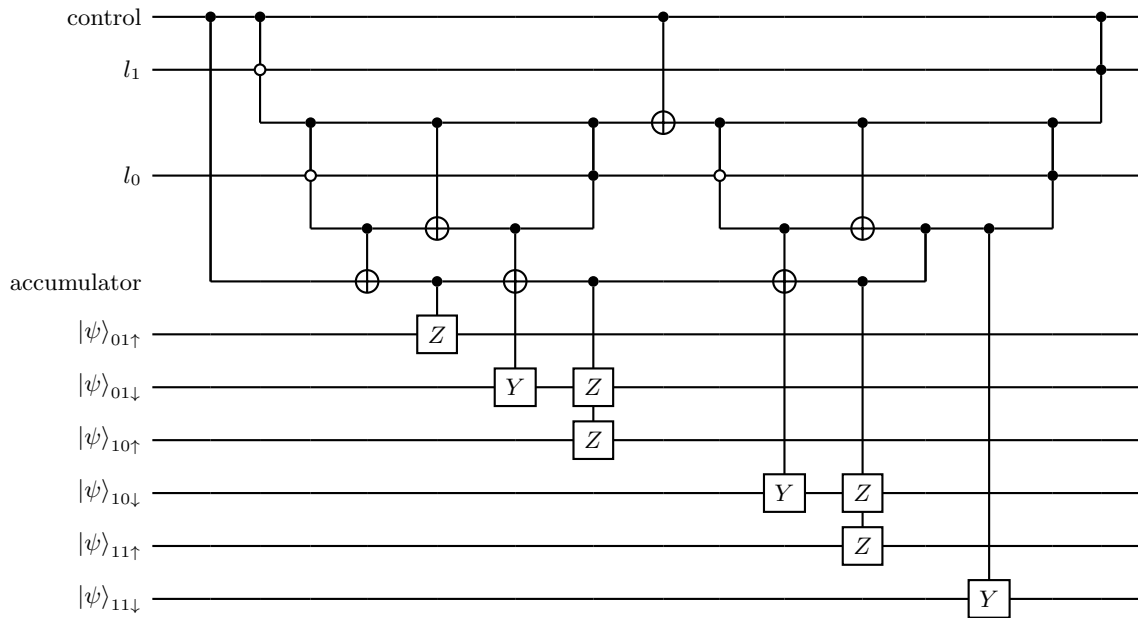
Conventional unary iteration circuits iterate over each individual qubit in a target register, with the index specifying which qubit to apply a gate to, or where to start/stop applying a Pauli string or similar gate to every qubit iterated over. We introduce a stride parameter k , allowing a unary iteration circuit to iterate over only $1/k$ of the qubits in a register (at $1/k$ the T -count) while still applying Pauli strings across every qubit in the register.

Additionally, we will include an index in our unary iteration that, instead of corresponding to a target qubit, corresponds to applying the operation to no qubits (that is, it corresponds to a NOOP). This is more efficient than adding a second control qubit to enable or disable the unary iteration, if the number of indices is not already a power of 2. We will label this index \emptyset .

Below, we construct example circuits for $(2)\text{In}_l$, the stride-2 unary iteration operator, applying Jordan-Wigner encoded Majorana operators on a register ψ of six qubits. These qubits are grouped as pairs addressed by $l \in \{01, 10, 11\}$, one representing the spin-up fermion and the other representing the spin-down fermion on each lattice site. Additionally, when $|l\rangle = |00\rangle$ the circuit performs NOOP; that is, we define $\emptyset = 00$.

For the spin-up case, $(2)\text{In}_l(\tilde{Z}Y_{l,\uparrow})$, we have

Similarly, for the spin-down $_{(2)}\text{In}_l \left(\vec{Z} Y_{l,\downarrow} \right)$, we have the circuit



This has a T -cost of $4L - 4$, just as for standard unary iteration, but here $L = \frac{N}{2} + 1$ for a T -count of $2N$ in contrast to the full (stride-1) indexed Majorana operator's $4N - 4$.